SKELETAL PHENOTYPE OF MICE LACKING HIP/RPL29, A COMPONENT OF THE LARGE RIBOSOMAL SUBUNIT

by

Daniel S. Oristian

A thesis submitted to the Faculty of the University of Delaware in partial fulfillment of the requirements for the degree of Master of Science with a major in Biological Sciences

Summer 2007

SKELETAL PHENOTYPE OF MICE LACKING HIP/RPL29

by

Daniel S. Oristian

Approved: _____
Catherine B. Kirn-Safran, Ph.D.
Professor in charge of thesis on behalf of the Advisory Committee

Approved: _____
Daniel D. Carson, Ph.D.
Chair of the Department of Biological Sciences

Approved: _____
Tom Apple, Ph.D.
Dean of the College of Arts and Sciences

Approved: _____
Carolyn A. Thoroughgood, PhD.
Vice Provost for Graduate and Research Studies

ACKNOWLEDGMENTS

I would like to thank my advisor, Dr. Catherine B. Kirn-Safran, for the constant support and guidance she has given me. I would not be the scientist today if it had not been for the opportunities she has provided for me.

I owe a great debt of gratitude to Dr. Cindy Farach-Carson. Her unrelenting passion for science and learning has been a great inspiration for me. From my undergraduate up through my graduate studies, she has been a great role model, teacher, and friend.

I would like to thank my committee members, Drs. Dan Carson and Jeff Twiss, for their guidance throughout my research and writing. Also I would like to acknowledge Dr. Liyun Wang, Dr. John Novotny, Dr. Kirk Czymmek, the Office of Laboratory Animal Management, the histology cores at A. I. DuPont Hospital for Children and at the University of Alabama at Birmingham, and the Center for Translation Cancer Research at the University of Delaware.

I would like to thank the entire Carson and Farach-Carson lab groups not only for teaching me the basic skills and techniques I needed to complete this work, but for providing me with moral support and encouragement that only true friends can provide.

To all of my friends here at Delaware and back home in Maryland, I could not have made it here without you. I would especially like to acknowledge my best friend, Jon Ward, for always being there, any hour of the day or night.

I would like to thank Kristi and Jamie Oristian, Kristina Hines, and Greg Dodson for being the best younger brothers and sisters a guy could have. I would like to especially like to thank my older brother and sister, Dave Oristian and Anastasia Arab, through all the highs and lows of my life, they have been there to pick me up when I have fallen and lifted me higher when I succeeded.

I wish to express my deepest appreciation to my parents Eric and Laurie Oristian and Rita and Russell Dodson. I would have never made it this far if it was not for the love and support you have given me. I am truly blessed to have you in my corner as I take the next steps in my life.

Finally, I would like to dedicate this work to my late grandfather Dr. Steven Oristian. He is, and always will be, the driving force in my life. The strength, love, and wisdom he instilled in me made me the man I am today. We will forever love and miss you.

TABLE OF CONTENTS

LIST OF TABLES vii
LIST OF FIGURES viii
LIST OF ABBREVIATIONS ix
ABSTRACT xii
Chapter 1 1
1.1 Skeletal bone development 1
1.2 Ribosome biogenesis and protein translation 5
1.3 Heparan Sulfate Interacting Protein/ Ribosomal Protein L 29 (HIP/RPL29) 8
1.3.1 Extra-ribosomal function of HIP/RPL29 9
1.3.2 HIP/RPL29: A component of translationally active ribosomes 10
1.3.3 Role of HIP/RPL29 during development and *in vitro* chondrogenesis 12
1.4 Creation of HIP/RPL29 null animals 13
1.5 Objectives 15
Chapter 2 16
2.1 Animal care and handling 16
2.2 Skeletal analysis 16
2.3 Micro computed axial tomography 17
2.4 General histology 18
2.5 Quantification of TRAP activity 19
2.6 Creation of PMEFs 19
2.7 *In vitro* proliferation assays 20
2.8 *In vivo* proliferation assay 20
2.9 Global protein synthesis assay 21
2.10 SDS-PAGE analysis 22
Chapter 3 24
3.1 Absence of HIP/RPL29 protein product in mice targeted at the *Hip/Rpl29* locus 24
3.2 Phenotype of HIP/RPL29 null mice 26
3.3 Characterization of the short stature phenotype in adult HIP/RPL29$^{-/-}$ mice. 28
3.4 Geometry of HIP/RPL29-deficient bones 30
3.5 Cellular effects of *Hip/Rpl29* gene disruption *in vivo* and *in vitro* 38
3.6 Lack of HIP/RPL29 impairs protein translation 41
Chapter 4 44
4.1 Global skeletal defects in HIP/RPL29 null mice 44
4.2 *In vivo* and *in vitro* cellular effects of HIP/RPL29 protein deletion 46
4.3 Protein translational efficiency was compromised in HIP/RPL29-deficent cells 48

4.4 Conclusions 50
REFERENCES 52

LIST OF TABLES

Table 1. Diaphyseal cortical parameters are significantly decreased in HIP/RPL29-deficient femurs...…..…….32

Table 2. Trabecular microstructure is maintained in HIP/RPL29 mice……..33

LIST OF FIGURES

Figure 1. HIP/RPL29 colocalizes with RPS6 and translationally active ribosome....11

Figure 2. *Hip/Rpl29* gene targeting strategy…….....14

Figure 3. Disruption of *Hip/Rp*l29 gene abolishes protein expression…….....25

Figure 4. Short stature phenotype of HIP/RPL29 null mice was apparent in pre- and postnatal life……..……..27

Figure 5. Whole body and individual bone measurements in Hip/Rpl29^{tm2Udel} null and control mice…….29

Figure 6. Decreased bone marrow area was apparent in both male and female HIP/RPL29-deficient mice……..31

Figure 7. Comparative histology of WT and HIP/RPL29-deficient femora…….....35

Figure 8. TRAP analysis of the growth plate of proximal tibiae……....36

Figure 9. Tibia growth plates of six-month-old female HIP/RPL29 null mice display shortened and well organized growth plates……...37

Figure 10. HIP/RPL29-deficient cells display decreased rates of *in vitro* proliferation…….39

Figure 11. Cell density was increased in the reserve zone of HIP/RPL29 null embryo distal femoral epiphyses……..40

Figure 12. HIP/RPL29 deletion resulted in reduction of core ribosomal components, decreasing overall translation……..43

LIST OF ABBREVIATIONS

ANOVA	one-way analysis of variance
BMC	bone mineral content
BMD	bone mineral density
BSA	bovine serum albumin
BrdU	bromodeoxyuridine
Bst	belly spot and tail
COX-2	cyclooxygenase -2
COOH	carboxy terminal
DNA	deoxyribonucleic acid
DMEM	Dulbecco's modification of Eagle's medium
ECM	extracellular matrix
eIF4A	eukaryotic initiation factor 4A
eIF4F	eukaryotic initiation factor 4F
eIF4G	eukaryotic initiation factor 4G
ES	embryonic stem cells
GTP	guanine triphosphate
HET	heterozygous
HIP/RPL29	heparan sulfate interacting protein/ribosomal protein L29
Hp	heparan
H_2O	water
HS	heparan sulfate

IF	initiation factor
KOH	potassium hydroxide
mRNA	messenger RNA
NBF	neutral buffered formalin
NH_2	amino
Nmd3p	nuclear export protein
P	proliferative zone
PBS	phosphate buffered saline
PCR	polymerase chain reaction
PIC	pre-initiation complex
PMEF	primary mouse embryonic fibroblasts
QPCR	quantitative PCR
R	reserve zone
RER	rough endoplasmic reticulum
RMRP	RNA component of mitochondrial RNA processing endoribonuclease
RNA	ribonucleic acid
RP	ribosomal protein
RPL10	ribosomal protein of the large subunit 10
RPL17	ribosomal protein of the large subunit 17
RPL24	ribosomal protein of the large subunit 24
RPL29	ribosomal protein of the large subunit 29
RPS6	ribosomal protein of the small subunit 6
RPS16	ribosomal protein of the small subunit 16
RPS19	ribosomal protein of the small subunit 19

ROI	region of interest
rRNA	ribosomal RNA
S6K	S6 kinase
SDS-PAGE	sodium dodecyl sulfate polyacrylamide gel electrophoresis
SEB	sample extraction buffer
TCA	tricholoracetic acid
TCOF1	Treacher Collins-Franceschetti syndrome 1
TOP	tract of polypyrimidines
TRAP	tartrate resistant acid phosphatase
tRNA	transfer RNA
t-test	statistical test
µCT	micro computed axial tomography
UTR	untranslated region
WT	wildtype

ABSTRACT

Ribosomal proteins (RPs) play important regulatory functions in the ribosome and modulate protein synthetic rates in response to external cues. Disruption of the *heparan sulfate interacting protein/Rpl29* (*Hip/Rpl29*) gene caused a global growth defect in homozygous null mutants, resulting in a short stature phenotype that is apparent from prenatal life through adulthood. In primary mouse embryonic fibroblasts, the absence of HIP/RPL29 is accompanied by a reduction in proliferation and protein synthesis, and a decrease in the steady state levels of core ribosomal components. Interestingly, the proliferation index of HIP/RPL29 null chondrocytes remains unaffected in developing growth plates suggesting that the skeletal growth defect might rather be a consequence of a deficiency in bone matrix synthesis. To investigate the postnatal effects of HIP/RPL29 absence on adult bone structure, I compared the wet weight of individual long bones (femur and tibia) in null mutants and control mice. I found that the average bone weight is approximately 30% lower in null animals when compared to corresponding bones in controls. I also evaluated the cortical and trabecular bone morphology differences between HIP/RPL29 null and control animals using standard histology and micro-computed tomography (micro-CT). We found that HIP/RPL29 null femoral diaphyses exhibit a significant decrease in bone marrow (40%) and cortical (15%) areas. In addition, a significant 30% decrease in the polar moment of inertia in HIP/RPL29-deficient bones was observed.

On the other hand, no significant differences were detected in the trabecular microstructure of the distal femur in null mice when compared to controls. Altogether, these data show that the amount of total bone tissue is decreased in mice lacking a regulatory component of the ribosome, supporting the idea that high volume protein synthesis is essential for bone matrix production during periods of rapid bone growth, predominantly during development. Stimulation of this pathway might provide novel means of accelerating bone and connective tissue regrowth during wound healing.

Chapter 1

GENERAL INTRODUCTION

1.1 Skeletal bone development

The vertebrate skeleton, composed of bone and cartilage, is the product of a tightly regulated differentiation of three distinct embryonic cell lineages: 1) cranial neural crest cells, 2) paraxial mesenchymal cells, and 3) lateral plate mesenchymal cells. This complex system requires the migration of these specific lineages to sites of bone formation and arrangement into high-density mesenchymal condensations (Aszódi et al., 2000, Olsen et al., 2000). Differentiation into either osteoblasts or chondrocytes then will initiate the beginning of intramembranous or endochondral ossification sites, respectively. Intramembranous ossification will be responsible for generating craniofacial elements, with endochondral ossification working in tandem to generate axial skeletal elements (vertebrae and ribs) and long bones (Aszódi et al., 2000).

Chondrogenesis is a carefully coordinated developmental process that constitutes a template for the axial and appendicular embryonic skeleton that will be converted to bone (Olsen et al., 2000). In the case of long bones, this process takes place via a multistep differentiation cascade that includes: 1) commitment of the chondroprogenitors to a chondrogenic fate; 2) proliferation and maturation, followed by the secretion of

chondrocyte-specific markers into the extracellular matrix (ECM), specifically type II collagen; 3) withdrawal from the cell cycle; 4) hypertrophic growth and secretion of more ECM components, such as type X collagen, followed by; 5) apoptosis. As chondrocytes enter this terminal differentiation pathway, the cartilage matrix will enlarge and the ECM laid down by these hypertrophic cells will begin to calcify in a process known as endochondral bone formation. In long bones, primary ossification centers will form within the cartilage anlagen, expanding in each axial direction, establishing growth plates in the proximal and distal epiphyses, which later will be responsible for long bone growth (Miller et al., 2003, Mundlos and Olsen, 1997).

During embryogenesis, limb development occurs in a proximo-distal sequence, with cartilage serving as the template for endochondral ossification. The bones that compose the hindlimb are produced in order through a process of bifurcations and segmentations, generating the femur, followed by tibia and fibula, and finally the phalanges (Mundlos and Olsen, 1997, Olsen et al., 2000). Calcifying cartilage within the rods will be removed by osteoclasts and bone is deposited by osteoblasts, followed by angiogenesis and blood vessel invasion prior to birth. Shortly after birth and vascularization, secondary ossification centers arise in the bone epiphyses; cartilage generated here will be responsible for generating articular cartilage, which remains intact and serves as protection for epiphyseal bone (Aszódi et al., 2000). The cartilaginous growth plate will extend and diminish; this will be completely replaced by bone by the

end of puberty. Defects in any of these developmental steps can lead to skeletal abnormalities.

As a physical structure, bone is a combination of rigid, highly disordered inorganic component supported by a soft, organized organic matrix. Together, these two components work in tandem to generate heterogenous bone, allowing bone to fulfill its primary responsibility of providing structural support for vertebrate animals (Fritsch and Hellmich, 2007; Gupta et al., 2005). However, bone has many other functions that include the storage and maintenance of biological minerals, protection of vital organs, and as a hinge for muscles, allowing motion (Dempster et al., 2006, Gupta et al., 2005). The major components of bone come together in a regulated fashion to generate two types of bone, cancellous and cortical bone. Cancellous bone is young, metabolically active bone, constantly undergoing modeling and remodeling in response to mechanical and developmental stimuli from loading and growth, respectively. Cortical bone, on the other hand, is an older, more compact bone and undergoes less remodeling than cancellous bone. The maturity level of the cortical bone determines the biomechanical properties of bone in response to strain or stress (Dempster et al., 2006, Gupta et al., 2005 Rho et al., 1998).

Bone has been divided into a structural hierarchy which acts in a cooperative manner to withstand deformation due to stretch or compaction, bending, and torsional strains (Dempster et al., 2006, Gupta et al., 2005, Rho et al., 1998). The hierarchy is

composed of five levels: 1) the macrostructure, which includes cancellous and cortical bone; 2) the microstructure (10-500μm), made up of osteons and trabeculae; 3) the sub microstructure (3-7μm), which includes Haversian canals and lamellae, mineralized cartilage; 4) the nanostructure (0.5μm) composed of parallel arrangements of collagen fibrillar structures; and 5) the sub-nanostructure (1 nm) a collection of mature hydroxyl apatite crystals embedded in an organic matrix of collagen type I and non-collagenous proteins. Components of each level come together in a cooperative and regulated fashion to generate the next level of the hierarchy, and through these interactions, make bone a heterogeneous, rigid structure (Gupta et al., 2005, Rho et al., 1998).

The success of the skeleton relies not only on the developmental cues controlled by genetic factors dictating bone architecture, but also on the success of the bone structural hierarchy in response to mechanical stimuli and stress. The interdependent contributions of each skeletal elements overall morphology and inherent mechanical properties, allow the skeleton to be a dynamic organ capable of providing structural support to vertebrate animals (Rho et al., 1998, Rubin and Rubin, 2006). Imperfections occurring during skeletal formation will ultimately cause disruptions not only in bone element organization and size, but also will have major impacts on bone microstructure affecting the bone's ability to resist fracture and deformation under high stress or load conditions.

Inherited diseases affecting the skeleton are diverse and highly complex. Skeletal defects can be placed into two different categories. Skeletal dysplasias (1) affect the epiphysis, metaphysis and/or diaphysis of the bone, resulting in disproportionate limb or axial shortening. Typically, dysplasias are a result of abnormal mesenchymal condensations and chrondrocyte proliferation and maturation. Dysostosis (2), on the other hand, do not affect all bone tissues, but specific skeletal elements with the rest being normal (Olsen et al., 2000).

Of particular interest to my colleagues and I are osteochondrodysplasias resulting from defects in collagenous and non-collagenous extracellular matrix composition (Olsen et al., 2000). Ribosomal proteins (RPs) are known to be important players in the protein-synthesizing machinery and modulate protein synthetic rates in response to external cues. In recent years, several chromosomal mutations in RPs or proteins involved in ribosome biogenesis have been associated with human birth defects with clinical features that include skeletal growth deficiencies and/or deformities (e.g., RPS19 in Diamond-Blackfan, RS6K in Coffin-Lowry, RMRP in Cartilage-hair hypoplasia, TCOF1 in Treacher Collins) (Liu and Ellis, 2006). These observations strongly link the fundamental processes of protein synthesis and skeletogenesis.

1.2 Ribosome biogenesis and protein translation

From human to yeast, the eukaryotic ribosome is composed of tightly conserved ribosomal RNAs (rRNA), RPs, and non-ribosomal factors, that assemble in a sequential

pattern leading up to a structurally and functionally conserved ultrastructure (Fatica et al., 2002, Tschochner and Hurt, 2003). rRNA supplies not only the basic framework for the ribosome, but also is responsible for the catalytic activity mandatory for peptide bond formation. RPs associated within the ribosome have been implicated in messenger RNA (mRNA) and transfer RNA (tRNA) recognition and the binding of GTP-containing translation factors. Individual RPs also serve as integral parts of the peptidyl-transferase center and exit tunnel of the ribosome and are required for nuclear export of ribosomal subunits into the cytoplasm (Brodersen and Nissen, 2005). Ribosome biogenesis is a very costly event for the cell, demanding high metabolic activity within the cell for high energy expenditures (Fromont-Racine et al., 2003, Tschochner and Hurt, 2003). Formation of ribosomes cannot occur spontaneously because of its dependence on the unified and tightly regulated action of RNA polymerases I, II and III to produce equimolar amounts of rRNAs, mRNAs for RPs and 5S rRNA, respectively, as well as rRNA processing enzymes.

Ribosome biogenesis has been extensively characterized in the yeast strain *Saccharomyces cerevisiae* and is believed to require the following steps: 1) coordinated synthesis of pre-rRNAs and RPs, 2) assembly of RPs and pre-rRNAs, 3) processing and modification of pre-rRNAs, 4) separation of the two pathways leading to the formation of the pre-40S and pre-60S subunits, 5) step-wise and dynamic formation of nuclear 40S and 60S pre-ribosomal particles, and 6) transport of mature pre-ribosomes from the nucleolus through the nucleoplasm and out into to cytoplasm for 80S ribosome formation

(Tschochner and Hurt, 2003). Any missing components should affect the overall conformation and integrity of individual 40S and 60S subunits and ultimately the completed 80S ribosome (Fromont-Racine et al., 2003, Fatica and Tollevey, 2003, Tschochner and Hurt, 2003). Improper structure of the ribosome due to defects in folding or rRNA processing ultimately affects subunit assembly and integrity, decreasing speed and accuracy (Wool, 1996). Thus, incompletely or poorly formed ribosomes will fall off transcript more frequently and disassemble resulting in reduced protein production.

Once in the cytoplasm, the 40S ribosomal subunit will form a 43S pre-initiation complex (PIC) with many initiation factors (IF), then eIF4F will deliver the PIC to a nascent mRNA transcript in the cytoplasm and bind near the 5′UTR to form the 48S initiation complex. This process is mediated through eIF4G, a multidomain, scaffolding protein, required to bind mRNA to the 40S subunit, deliver eIF4A helicase to unwind secondary structure of mRNA transcripts, and maintain the transcript in a circular conformation through its interactions with cap and tail binding proteins on the mRNA (Raught et al., 2000). After the 5′UTR is scanned and the translation start site codon is recognized, a GTP-hydrolysis reaction takes place to form a translationally competent 80S ribosome (DeLabre et al., 2002).

The protein biosynthethic pathway is controlled by two factors, ribosome assembly and initiation of translation. In this regard, translation initiation is believed to be the rate-limiting step in this process and not ribosome content or assembly, because

assembly of ribosomes only occurs at the onset of translation initiation through the coordinated interactions of ribosomal subunits and translation IFs (Schmidt, 1999). Without the proper proteins or amounts of proteins, typical cell functions become compromised. Growth control relies on the regulated proliferation of cells; this process not only requires synthesis of DNA, but an increase in cell proteins and macromolecules to carry out these functions. Increasing protein synthesis requires accurate formation of ribosomal subunits and 80S ribosome assembly. Therefore, any defects in the maturation and export of pre-ribosomal subunits and formation in the cytoplasm will decrease overall protein production. Translation arrest, cell cycle arrest, and reduced growth are common characteristics of yeast strains or mammalian cell lines displaying defects in specific steps of ribosome biogenesis (DeLabre et al., 2002, Kispal et al., 2005, Pestov et al., 2001, Schmidt, 1999, Dong et al., 2004)

1.3 Heparan Sulfate Interacting Protein/ Ribosomal Protein L 29 (HIP/RPL29)

Murine HIP/RPL29 is a highly basic RP, composed of 160 amino acids with an apparent molecular weight of 28 kDa on SDS-PAGE, found exclusively in eukaryotes. Due to its many lysine residues, it is polycationic in nature and has been shown to selectively bind heparin/heparan sulfate (Hp/HS) chains of proteoglycans (Rohde et al., 1996). The murine polypeptide is 84% similar to the human ortholog and there is a strong conservation of the genomic structure as well (Hoke et al., 1998, Kirn-Safran et al., 2002). A high conservation of the NH_2-terminal portion of the protein exists across

phyla including Drosophila, yeast, and plants, with an absence of an elongated COOH-terminal region seen in mammals. Like many other RPs, the *Hip/Rpl29* mRNA transcript contains a sequence known as a 5′ tract of oligopyrimidines (TOP), and is driven by a TATA-less promoter (Kirn-Safran et al., 2000).

1.3.1 Extra-ribosomal function of HIP/RPL29

Wool (1995) suggested that during evolution many RPs have been recruited to the ribosome to stabilize its structure and enhance translation, but still retain extra-ribosomal functions. Evidence has accumulated to shown HIP/RPL29 has retained some secondary extra-ribosomal functions in humans and mice. It was identified on the cell surface of human epithelial cells, where it was shown to bind HS chains (Rohde et al., 1996) and act as an antagonist of heparanase-1 by blocking enzyme specific cleavage sites (Marchetti et al., 1997). In this context, HIP/RPL29 is believed to modulate the binding and release of heparin-binding growth factors from HS chains on the cell surface and in the ECM. *In vitro*, HIP/RPL29 supports HS-dependent cell adhesion and it also has domains capable of modulating anticoagulant activities of heparin (Liu et al., 1997). Finally, HIP/RPL29 has been shown to play a role in embryo adhesion at the embryo-uterine interface in a HS-dependent fashion through interaction with HS proteoglycans (Costell et al., 1999; Farach et al., 1987, Rohde et al., 1998).

1.3.2 HIP/RPL29: A component of translationally active ribosomes

HIP/RPL29 has been shown to be a component of translationally active ribosomes (Kirn-Safran et al., 2007). Immunocytochemistry performed on primary mouse embryonic fibroblast (PMEFs) demonstrated that HIP/RPL29 and the active, phosphorylated form of RPS6 of the small ribosomal subunit co-localize in the cytoplasm and along the rough endoplasmic reticulum (Fig. 1A and 1B). HIP/RPL29 also was found to be associated with ribosomes in the polysomal fractions using discontinuous sucrose gradients (Kirn-Safran et al., 2007). However, since HIP/RPL29 does not have a prokaryotic ortholog, it cannot be an essential part of the general translational machinery and is most likely to function as an accessory protein. *In vitro* cross-linking experiments indicate that HIP/RPL29 occupies a position at the interface between the two ribosomal subunits where it can potentially interact with RPs of the large and small subunits, tRNA, initiation factors, and mRNA (Nika and Nilsson, 1984). Therefore, HIP/RPL29 may potentially stabilize RNA-protein interactions and might increase ribosome translational efficiency in actively translating cells.

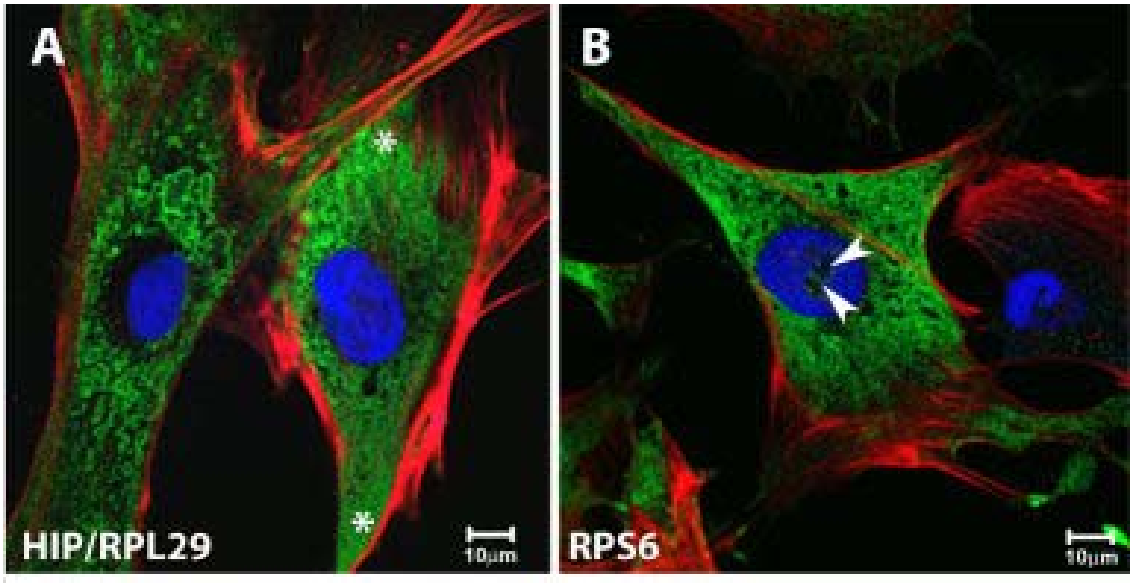

Figure 1: HIP/RPL29 co-localizes with RPS6 A) WT PMEFs isolated from day 14.5 mouse embryos show strong levels of HIP/RPL29 (green) in the cytosol and along the surface of the rough endoplasmic reticulum (RER). **B)** Phosphorylated RPS6 (green) show similar cytosolic and RER distributions when compared to cells labeled with antibodies directed against HIP/RPL29. Arrows show nuclear localization of RPS6 (Red: filamentous actin; Blue: nucleus). Adapted from Kirn-Safran et al., 2007.

In *Saccharomyces cerevisiae*, RPL29 was demonstrated to be a non-essential gene that encodes a component of the 60S ribosomal subunit (DeLabre et al., 2002). In this system disruption of RPL29 expression lead to delayed *in vitro* growth associated with a lag in translation initiation, followed by a 50% decrease in the rate of protein synthesis. Absence of RPL29 was accompanied by deficient assembly of proteins into ribosomal subunits and an impaired loading of the 40S subunit onto the large 60S ribosomal, indicated by half-mer polysomes. Overexpression of RPL10 in the RPL29 deletion strains corrected the ribosome biogenesis defect. RPL10, like RPL29, occupies a

position on the inner cleft of the large ribosomal subunit and is believed to interact with the small subunit during 80S assembly. It is, therefore, suggested that addition of RPL29 late in ribosome assembly aids in the attachment of RPL10 and Nmd3p, a nuclear export protein part of the nuclear export complex, to the large ribosomal subunit, respectively. Attachment of nuclear export proteins will allow for the subsequent export of the 60S subunit from the nucleus to the cytoplasm (Hedges et al., 2005). Once RPL29 and RPL10 are attached to the mature 60S subunit, they will interact with the small 40S subunit-mRNA complex and stabilize the bridging of the two subunits, generating a complete 80S subunit (DeLabre et al., 2002).

1.3.3 Role of HIP/RPL29 during development and *in vitro* chondrogenesis

HIP/RPL29 displays a much more prevalent pattern of expression throughout embryonic development when compared to differentiated adult tissue, and high levels of HIP/RPL29 have been also found in all developing organs (Kirn-Safran et al., 2000; Julian et al., 2001). It has been demonstrated that HIP/RPL29 also serves as a marker for abnormal growth when overexpressed, and there is an increase in its expression in human carcinomas (de Nigris et al., 1998; Wang et al., 1999). In the developing long bones of the mouse embryo, HIP/RPL29 expression is found primarily in proliferating cartilage and is greatly reduced in terminally differentiated chondrocytes. Ribozyme-mediated knockdown of HIP/RPL29 transcripts in a multipotent chondroprogenitor cell line subsequently resulted in premature differentiation into chondrocyte-like cells (Miller et al., 2003).

Chondrogenesis and endochondral bone formation requires an increase in protein synthesis to aid in the proliferation and synthesis of matrix proteins (Olsen et al., 2000). Cellular processes in the bone microenvironment control both the distribution and organization of bone tissues responsible for the maintenance of bone structure and development (Rubin and Rubin, 2006). These cellular processes require high levels of protein expression. Therefore, investigation of the mechanisms controlling protein biosynthesis may aid in the understanding and treatment of musculoskeletal disorders characterized by abnormal levels of protein production, such as Coffin-Lowry Syndrome (Yang et al., 2004) and Treacher Collins Syndrome (Dixon et al., 2006)

1.4 Creation of HIP/RPL29 null animals

Using a homologous recombination targeting strategy in mouse 129S6 embryonic stem (ES) cells, the *Hip/Rpl29* gene was disrupted by replacement of the first three exons with a neomycin selection cassette (Fig. 2). Targeted ES cells were isolated and microinjected into developing blastocysts isolated from C57BL6/J mice, followed by transfer into pseudopregnant mothers. Resulting chimeras were bred to wild-type (WT) 129S6 inbred mice to generate HIP/RPL29 heterozygous (HET) mutants. Heterozygous male and females mice then were crossed, producing HIP/RPL29 WT, HET, and null progeny. HIP/RPL29 null mice were identified by Southern blot analysis to confirm the absence of the three first exons of the native *Hip/Rpl29* gene (Kirn-Safran et al., 2007).

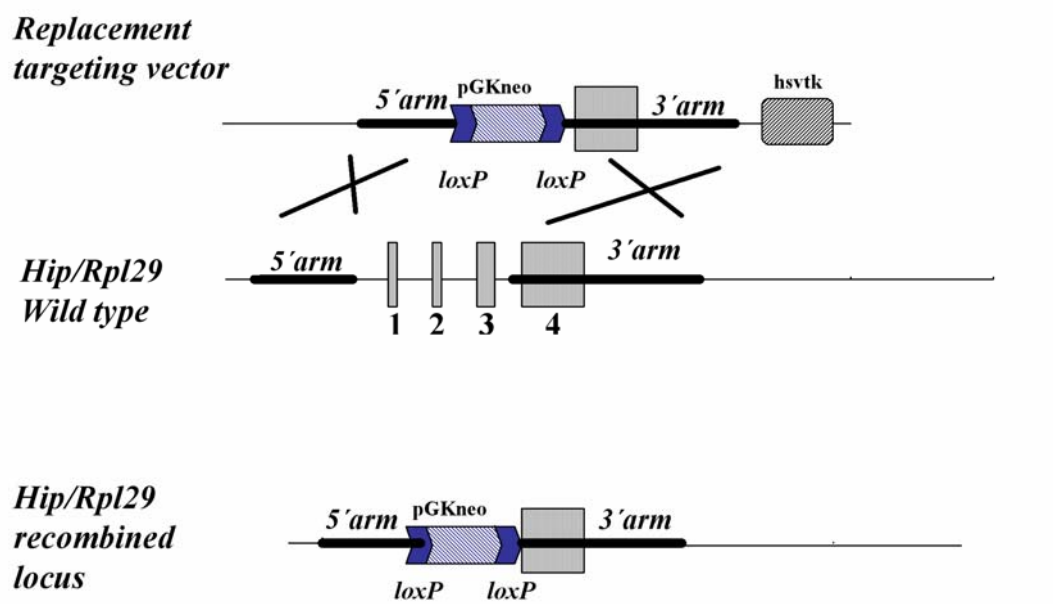

Figure 2: *Hip/Rpl29* gene targeting strategy. Disruption of *Hip/Rpl29* gene was achieved through homologous recombination with a HIP/RPL29 targeting vector. The first three exons of the gene were replaced by a neomycin selection cassette; this cassette was floxed by two loxP sites for removal of the neomycin cassette after using a Cre-loxP recombination system (Adapted Kirn-Safran et al., 2007).

Global growth deficiencies in mice lacking the ribosomal protein HIP/RPL29 are apparent during pre and post-natal development in two inbred mouse strains, 129S6 and C57Bl6/J. *In utero*, smaller body weights in HIP/RPL29 animals became apparent around mid-gestation. Developmental delays were observed in different types of tissues, specifically during digit septation and incisor eruption. Reduced placental size was also observed, suggesting delays seen in these mice may be related to placental insufficiency.

Substantial developmental retardations, including low birth weight and decreased organ and body size were characteristics in all null neonates (Kirn-Safran et al., 2007).

Embryonic delays observed in HIP/RPL29 null mutants seriously impact postnatal life. Postnatal lethality occurred in approximately 50% of the null progeny. Adult HIP/RPL29 deficient mice are subfertile, reach sexual maturity later and never match the length or weight of their non-mutant littermates.

1.5 Objectives

In view of this information, it was hypothesized that HIP/RPL29 supports rapid skeletal growth by playing a positive role in protein translation efficiency and subsequent ECM protein production. To test this hypothesis, three specific aims have been addressed:

I. Compare *in vivo* skeletal characteristics of control and HIP/RPL29-null mice.
II. Investigate effects of HIP/RPL29 absence during osteogenesis
III. Analyze global protein synthesis in WT and HIP/RPL29 null primary mouse embryonic fibroblasts.

Because of HIP/RPL29's participation in the process of ribosomal biogenesis, reduced rates in proliferation and global protein synthesis were anticipated. In addition, visual inspection of viable HIP/RPL29 null animals, led us to predict global long bone shortening rather than skeletal deformities.

Chapter 2

MATERIALS AND METHODS

2.1 Animal care and handling

Hip/Rpl29^{tm1Udel} and *Hip/Rpl29*^{tm2Udel} mice were generated as described (Kirn-Safran et al., 2007). All animal handling experiments and animal care were in accordance with the University of Delaware Institutional Animal Care and Use Committee approved guidelines.

2.2 Skeletal analysis

Skeletal preparations were performed on newborn mice of the 129S6 coisogenic background obtained from a *Hip/Rpl29*^{tm1Udel} heterozygous mating as described (Nagy et al., 2003) with minor modifications. Briefly, after euthanasia and removal of skin tissue and internal organs, including the eyes, carcasses were fixed overnight in 1% (v/v) acetic acid/95% (v/v) ethanol in H_2O and stained with Alcian blue (0.015% (w/v) (Sigma-Aldrich, St. Louis, MO.) /20% (v/v) acetic acid in 95% (v/v) ethanol) for 72 hrs. Skeletons then were dehydrated in 95% (v/v) ethanol for 24 hrs and placed in 1% (w/v) KOH until bone was visible. Finally, skeletons were stained overnight with Alizarin red

(Sigma-Aldrich) (15mg/100mL in 1% (w/v) KOH) and destained for 1 week in a 20 % (v/v) glycerol/1 % (w/v) KOH solution. For the analysis of the adult skeleton, six month-old male and female 129S6/C57BL6/J mix background *Hip/Rpl29*^{tm2Udel} null and control mice were sacrificed, weighed, and measured from anus to nose. Left and right femurs and tibias were isolated, stripped of excess tissue, weighed, measured, and fixed in 10% (v/v) neutral buffered formalin (NBF). Statistical analysis was performed using a two-tailed student's t-test.

2.3 Micro computed axial tomography

Intact male femurs from 129S6/C57BL6/J mixed background HIP/RPL29^{tm2Udel} mice were scanned wet, wrapped in a moist towel, and at a resolution of 27μm using a GE Healthcare eXplore Locus Pre-Clinical *in vivo* Micro-CT Scanner ® (GE Healthcare, North America). Images were reconstructed using GE's reconstruction utility and measurements were compiled and analyzed using GE's Microview ® software. For cortical measurements the mid-diaphysis was defined by selecting a 2mm segment at the midpoint between the proximal and distal femoral heads. A 3mm×3mm×2mm (X×Y×Z) region of interest (ROI, yellow in Fig. 4) was segmented at the mid diaphysis of the femur by using the autothreshold function of Microview ®. This allowed for the separation of mineralized and non-mineralized voxels obtained in the region of interest (Ling et al., 2005). The geometric measurements obtained were total cortical and bone marrow areas, bone mineral density (BMD), and bone mineral content (BMC). The polar

moment of inertia was calculated as described (Koller et al., 2003). Trabecular data was collected from a free form ROI generated 250μm below the distal growth plate using the stereology feature of the Microview ® Software. Statistical analysis was performed using unpaired two-tailed student's t-test.

2.4 General histology

For analysis of the cortical region in six-month old females, femural bones from HIP/RPL29^{tm2Udel} 129S6/C57BL6/J mixed background mice were harvested and fixed as described above. The femurs were embedded in polymethylmethacrylate and sectioned into 300μm-thick sections using a diamond saw. Femurs and tibias from six month-old control and null HIP/RPL29 females also were sent to the University of Alabama-Birmingham for embedding, sectioning, and staining courtesy of Dr. Majd Zayzafoon. Femurs were embedded in polymethylmetacrylate and tibias were decalcified and embedded in paraffin. Sections of femurs (5μm) were obtained and subjected to Von Kossa and Goldner's Trichrome staining techniques as described (Kline, 1955, Yeo et al., 2007). Sections obtained from the tibia were tested for tartrate-resistant acid phosphatase (TRAP) enzymatic activity as described (Yeo et al., 2007). Hematoxylin and eosin staining was obtained on consecutive sections using a standard histology procedure.

2.5 Quantification of TRAP activity

Images of the tibia proximal growth plate were analyzed as described in Sawyer et al. (2003) with modifications. Images were taken under a magnification of 40x using Zeiss Akioskop 2 (Carl Zeiss Inc., Oberkochen, Germany) and SPOT ® Advanced imaging software and camera (Diagnostic Instruments Inc., Sterling Heights, MI.). All images were captured at the same light intensity, gain, and balance to ensure constant illumination conditions; resulting images were reconstructed using Adobe Photoshop 7.0 ® (Adobe Systems Incorp. San Jose, CA.). A 10μm^2 area was generated in the center of the growth plate, including the bottom portion on the calcified growth plate and upper limits of the primary spongiosa by placing five circles with a diameter of 150 pixels in a series along the curvature of the growth plate. All circles where combined to generate a 10 μm^2 area (see oval in Fig. 8A); the total number of pixels was calculated for this area. Using the color-picking function in Adobe Photoshop, TRAP activity was identified and segmented from the tissue and background. The total number of pixels corresponding to TRAP activity where then quantified using Zeiss AIM LSM 510 (Rel 4.2) imaging software (Carl Zeiss). TRAP quantification was reported as the number of TRAP positive pixels relative to the total pixels in the 10μm^2 region of interest. Statistical analysis was performed using unpaired two-tailed student's t-test.

2.6 Creation of PMEFs

PMEFs cultures were isolated from day 14.5 embryos obtained from the heterozygous mating of *Hip/Rpl29*^{tm1Udel} mice of a 129S6 background. Individual embryos were dissected away from uterine tissue and extraembryonic membranes, including the

placenta as described (Robertson, 1987). Following removal of the head and viscera, carcasses were finely minced and digested with trypsin. Cells then were plated onto a gelatinized 10-cm Petri dish with medium, including DMEM (Invitrogen, San Francisco, CA.), 10% (v/v) fetal bovine serum (Hyclone, Logan, UT.), 2mM L-glutamine (Invitrogen), 10^{-4} β mercaptoethanol (Sigma-Aldrich), and penicillin and streptomycin at 50μg/mL each. A PCR based method was employed to determine genotypes of isolated cell lines as described (Kirn-Safran et al., 2007).

2.7 *In vitro* proliferation assays

To analyze cell proliferation, wildtype, heterozygous, and null PMEFs were plated at a density of 5×10^3 cells per well of a 96-well dish. Twenty-four hours later, individual wells were incubated with a tetrazolium salt (WST-1) (Roche, North America) and every other day thereafter. The number of metabolically active cells present in the culture was quantified by measuring the appearance of formazan, a water-soluble cleavage product of mitochondrial dehydrogenases, at an absorbance of 450 nm after a reaction period of 90 min. Experiments were conducted using quadruplicate samples and were repeated twice.

2.8 *In vivo* proliferation assay

Day 18.5 pregnant mothers were injected intraperitoneally with 100μg bromodeoxyuridine (BrdU)/per gram body weight (Sigma-Aldrich). Two hours later the females were sacrificed and embryos were collected. Hindlimbs were isolated and fixed in 10% (w/v) neutral buffered formalin (NBF) and processed for paraffin embedding and

sectioning. Sections (5μm) were deparaffinized and immunostained using ZYMED BrdU Staining Kit ® (Invitrogen) for BrdU incorporation or counterstained with Safranin O and Fast Green. Distal femoral epiphyses/growth plates were analyzed for number of BrdU-positive cells/40 μm^2 area using Image J ® image analysis software (NIH, Bethesda, MD). Briefly, slides were immersed in Safranin O (Sigma-Aldrich) for 1 hr, washed in running water and passed through a series of graded alcohol under agitation. Slides were then stain with alcoholic Fast Green FCF (Sigma-Aldrich), rinsed with alcohol, cleared with two changes of Citrisolv ® (Fisher Scientific, North America) and mounted using a resinous mounting medium, Cytoseal ® 60 (Richard Allan Scientific, Kalamazoo, MI.). Statistical analysis was performed using unpaired two-tailed student's t-test

2.9 Global protein synthesis assay

To investigate the rates of global protein synthesis, wildtype and HIP/RPL29 null PMEFs were plated and grown to subconfluency in six-well plates, washed with PBS, and supplied with cell culture medium without cysteine and methionine (Invitrogen) for 45 minutes. PMEFs then were labeled for 3hrs using cell culture medium supplemented with [^{35}S] cysteine/[^{35}S] methionine mixture (GE Healthcare) at a final concentration of 0.5 mCi/mL per well. Cells then were washed two times with PBS and lysed in 55μL of sample extraction buffer (SEB) containing 0.05 M Tris pH 7.0, 8 M urea, 1% [w/v] SDS, 1% [v/v] β-mercaptoethanol, and 1% [v/v] protein inhibitor cocktail (Sigma-Aldrich); debris was cleared from cell lysates after a 13,000 rpm spin for 20 min at 4°C. An

aliquot of 10 μL was used to quantify protein concentration as described (Lowry, 1951). From the remaining sample, 10μL were precipitated in 20% (w/v) tricholoracetic acid (TCA) to test for [^{35}S] cysteine/[^{35}S] methionine incorporation. Precipitates then were spotted on 1.5 cm GF/C filters (Whatman, Brentford, UK), washed three times with 5% (w/v) TCA and twice with absolute ethanol. Filters were allowed to air dry and were placed into scintillation vials containing Opti-Fluor (Packard Bioscience, Meridan, CT.) and counts per minute (cpm) were acquired by a liquid scintillation analyzer (Packard Bioscience). Global protein synthesis rates were determined by dividing the TCA-precipitable cpm by the total amount of protein present in the sample. Statistical analyses were performed using ANOVA followed by a Tukey-Kramer secondary multiple comparison test.

2.10 SDS-PAGE analysis

Day 18.5 embryonic tissues were ground in a liquid nitrogen-cooled mortar and homogenized in a 1-mL Dounce homogenizer for 20 strokes in sample extraction buffer (SEB, described above). PMEF samples were collected by direct solubilization in SEB in which a phosphatase inhibitor cocktail (Calbiochem, North America) was added at 1% (v/v) concentration. Protein samples were quantified using the Lowry Assay (Lowry, 1951) and equal amounts of protein lysates (10-20μg) were combined with 2x Laemmli buffer (Bio-Rad, Hercules, CA.) and subjected to 10% (w/v) SDS-PAGE as described (Julian et al., 2001). After transfer to a nitrocellulose membrane, the blots were blocked in blocking buffer (5% [w/v] BSA, 0.1% [v/v] Tween-20 in PBS or 3% [w/v] nonfat dry

milk, 0.1% [v/v] Tween-20 in PBS) for at least 6 hr and probed with specific antibodies raised in rabbit. Primary antibody dilutions in blocking buffer and incubation times were as follows: 1:5,000 (v/v) polyclonal anti-HIP/RPL29 peptide 43-53 (FAKK) for 1 hr (Hoke et al., 1998); 1:3000 (v/v) polyclonal anti-HIP/RPL29 peptide 2-25 for 1 hr; 1:10,000 (v/v) anti-full-length recombinant HIP/RPL29 for 1 hr; 1:2,000 (v/v) monoclonal anti-RPS6 for 12 hr (Cell Signaling, Boston, MA); 1:1000 (v/v) anti-phosphorylated S6 (235/236) 12 hr at 4^{o}C; 1:2000 (v/v) anti-phosphorylated S6 (240/244) for 12 at 4^{o}C; 1:1000 (v/v) anti-S6 Kinase (Cell Signaling) for 12 hr at 4^{o}C; 1:1000 (v/v) anti-eIF4G (Cell Signaling) for 12 hr at 4^{o}C; 1:1000 (v/v) anti-phosphorylated eIF4G (Cell Signaling) 12 hr at 4^{o}C; and 1:500 (v/v) anti-RPL17 for 12 hr (Laine et al., 1991, Zheng et al., 2001). After three washes in PBS/0.1% (v/v) Tween-20, the blot was incubated with a 1:200,000 (v/v) dilution of horseradish peroxidase-conjugated anti-rabbit IgG secondary antibody (Sigma). Detection was performed using the West Dura® Super Signal detection kit (Pierce, Rockford, IL). Blots then were reprobed with a 1:15,000 (v/v) dilution of monoclonal rabbit anti-β-actin antibody (Abcam, Cambridge, MA) in 5% BSA (w/v) blocking buffer as described above. Signal intensities were quantified using densitometry software of the Alpha Imager (Alpha Innotech Corp., San Leandro, CA.).

Chapter 3

RESULTS

3.1 Absence of HIP/RPL29 protein product in mice targeted at the *Hip/Rpl29* locus

To confirm knockout of the *Hip/Rpl29* gene, Western blot analysis was carried out on protein extracts from wild-type, heterozygous, and homozygous animals. Using an antibody directed against a peptide sequence unique to HIP/RPL29 functional protein (anti-FAKK peptide [43-53]), (Fig. 3A), I was able to confirm a complete absence of the resulting gene product (Fig. 3B). Further analysis of protein extracts by Western blot with two other antibodies directed against either the NH_2-terminal portion of the protein product (Anti-peptide 2-25, Fig. 3A) or the entire HIP/RPL29 polypeptide (HIP/RPL29 full-length recombinant) further confirmed a knockout of the total protein (Fig. 3C). Heterozygous animals displayed an intermediate level of HIP/RPL29 protein expression, when compared to wild-type and null mice (data not shown).

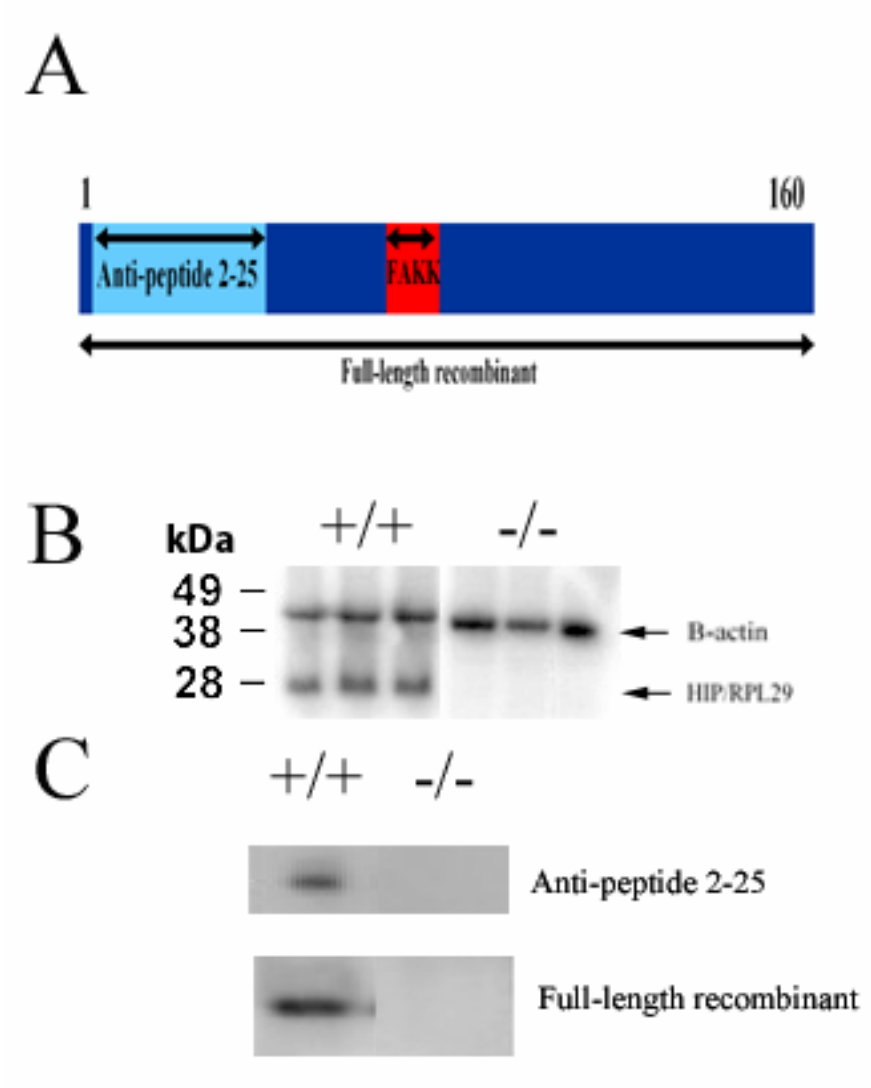

Figure 3: Disruption of Hip/Rpl29 gene abolishes protein expression. Three antibodies directed against different regions of HIP/RPL29 polypeptide were used to confirm knockout of the protein product (A). Western blot analysis of day 18.5 embryo extracts using FAKK antibody (B). Antibodies directed against the NH2-terminal portion of HIP/RPL29 and the full-length recombinant also were used on day18.5 embryo extracts(C).

3.2 Phenotype of HIP/RPL29 null mice

Prior to birth, HIP/RPL29 mice displayed a global short-stature phenotype throughout all stages of development. Delay in embryonic development was apparent in prenatal HIP/RPL29 embryos (day 17.5) and one-week-old mice (Fig. 4A&C). Whole skeleton analysis of newborn null HIP/RPL29 mice by Alizarin red and Alcian blue staining reveal no specific defect in the patterning of cartilage and bone elements (Fig 4B). Closer analysis of newborn limbs showed a reduction in hindlimb lengths and a delay in the mineralization of bones in the phalangeal, metatarsal, talus, and calcaneous bones of the foot (Fig. 4D).

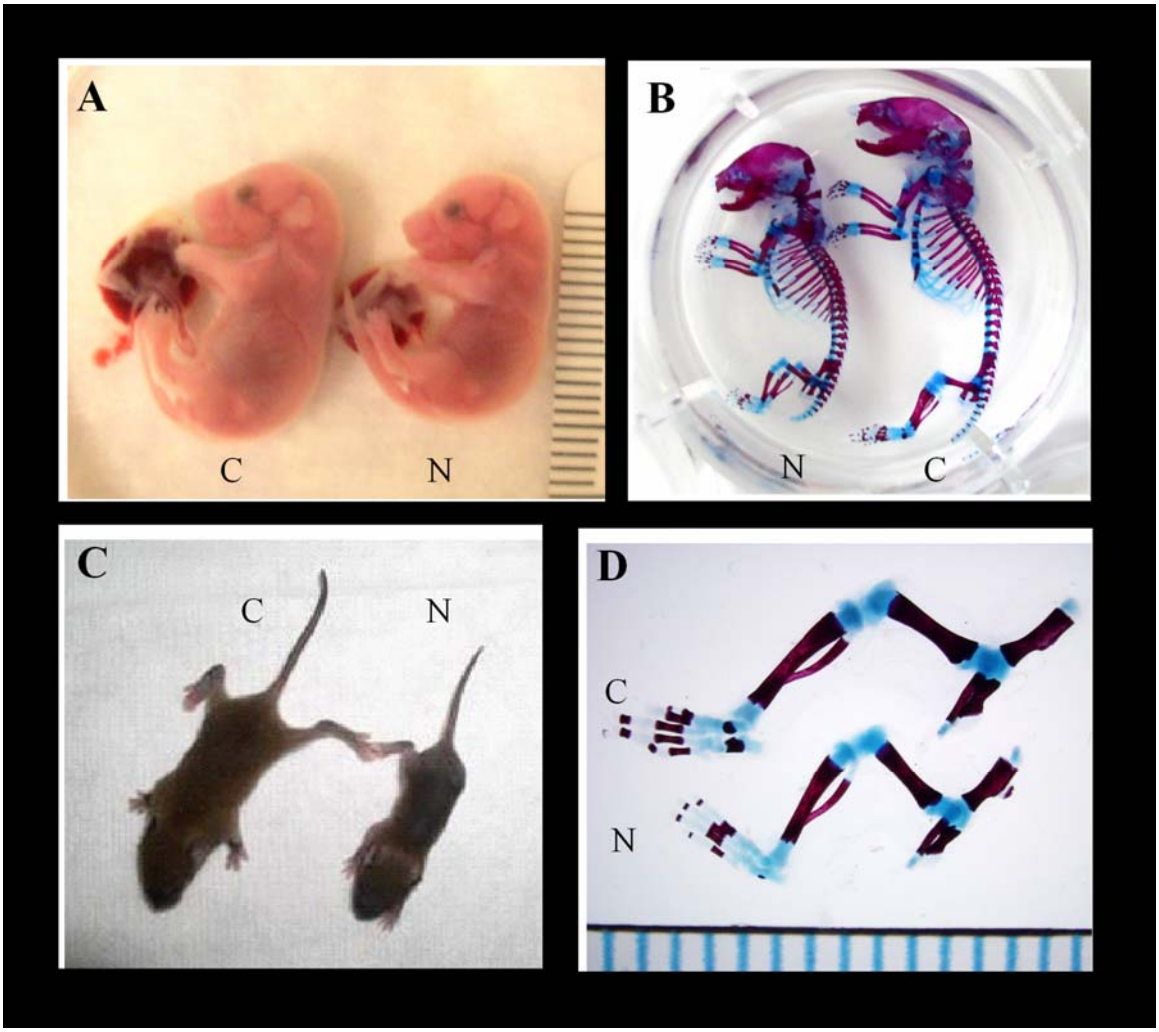

Figure 4: Short stature phenotype of HIP/RPL29 null mice was apparent in pre- and postnatal animals. Delay in development was apparent in prenatal HIP/RPL29 null embryos (day 17.5) and one-week-old mice (**A&C**). Null HIP/RPL29 postnatal mice did not display any gross skeletal abnormalities, but showed a reduction in axial and appendicular bone length (**B**) and delayed mineralization in bone extremities as illustrated in the foot (**D**). Adapted from Kirn-Safran et al., 2007.

3.3 Characterization of the short stature phenotype in adult HIP/RPL29$^{-/-}$ mice.

HIP/RPL29 null mice continued to display a global growth defect throughout adulthood on both mixed and inbred genetic backgrounds (Kirn-Safran et al, 2007). Six-month old male and female mice harboring the *Hip/Rpl29*^{Udeltm2} mutation, in which the neomycin selection cassette was removed, on a 129S6/C57BL6/J mixed background continued to display the short stature phenotype. Total body length in both males and females was reduced approximately by 10% when compared to control animals (Fig. 5A $p<0.001$). Interestingly, both male and female HIP/RPL29 nulls displayed a reduced overall body weights at 25% ($p<0.005$) and 30% ($p<0.001$) with respect to controls, respectively (Fig. 5B). Further measurements taken of individual bones isolated from null mice indicated a decrease in total length when compared to control bones of the same age (Fig. 5C). This reduction in size was accompanied by an approximate 30% decrease in the corresponding wet weight of both femurs and tibiae (Fig. 5D, $p<0.001$ null vs. control).

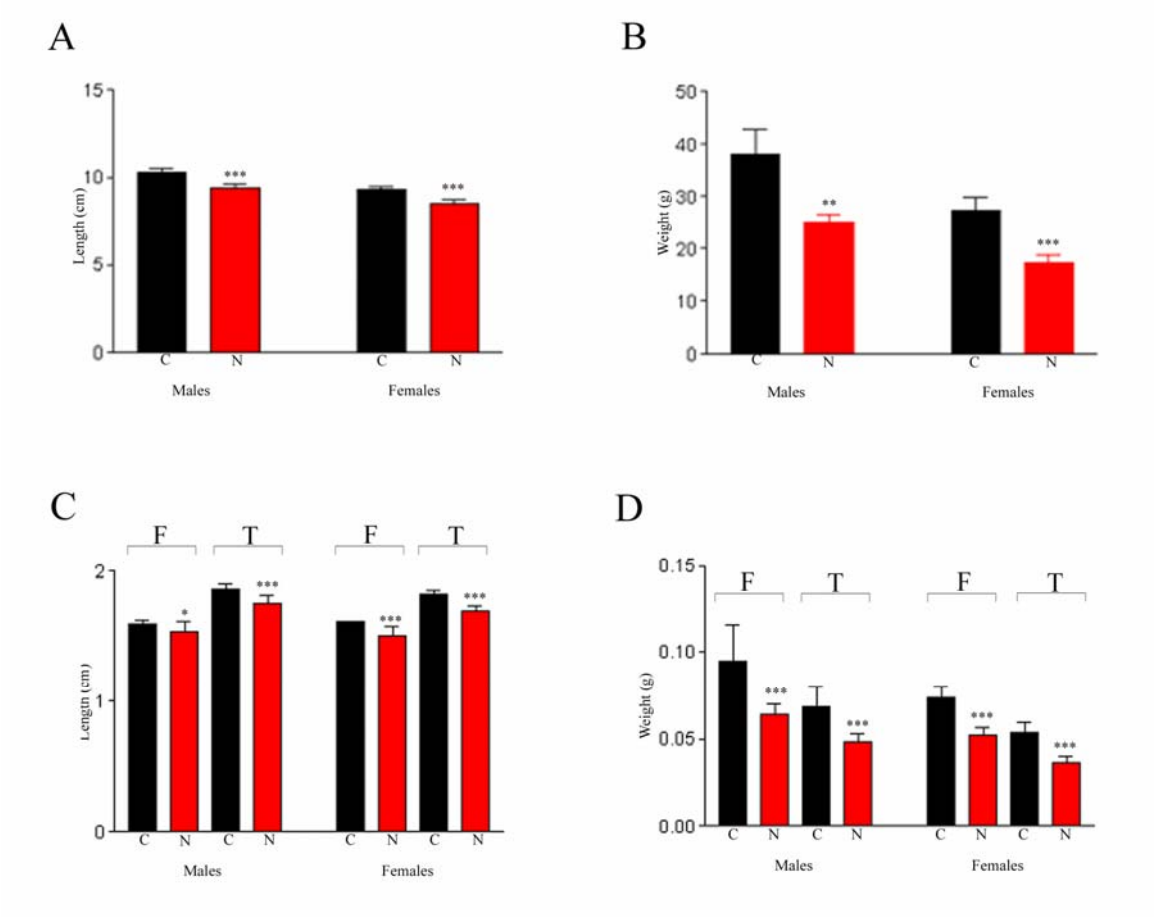

Figure 5: Whole body and individual bone measurements in *Hip/Rpl29*^{tm2Udel} null and control mice. Measurements of HIP/RPL29 null mice (N) showed a 10% and a 30% decrease body length (**A**) and in total weight (**B**), respectively, when compared to controls (C). Further analysis of individual long bones (F=femur, T=tibia) of null mice also showed an estimated 30% decrease in wet bone weight **(D)**. Overall bone length was only decreased by less than 7% in HIP/RPL29-deficient bones **(C)**. ***, ** and * denote a statistically significant difference ($p<0.001$, $p<0.005$, and <0.05, respectively) in HIP/RPL29-deficient mice relative to wild type**.**

3.4 Geometry of HIP/RPL29-deficient bones

The microstructure of HIP/RPL29-deficient long bones was analyzed by micro computed tomography (μCT) and standard histology techniques as described in Materials and Methods. Radiographs of the femur of control (Fig. 6A) and HIP-RPL29-deficient male mice (Fig. 6B) revealed a decrease in bone marrow area at the mid diaphysis in mutant animals. The same observation could be made when comparing cross-sections of age matched control and null female femurs (Fig. 6C&D). Cortical measurements taken at the midshaft (see yellow area Fig. 6) of adult male femurs (Table 1) confirmed a significant reduction in the inner and outer perimeter of HIP/RPL29 null vs. control bones, which resulted in a 39.7% ($p<0.05$) and 15.1% ($p<0.05$) decrease in marrow and cortical areas, respectively. The calculated polar moment of inertia, which gives insight into the relative distribution and amount of torsional strain a structure can withstand, was significantly decreased in HIP/RPL29-deficient bones when compared to control bones ($p<0.05$). Surprisingly, there was no apparent difference in the bone mineral density (BMD) or bone mineral content (BMC) between null and control mice at six months of age. Analysis of trabecular microstructure in the femoral heads 250μm below the established growth plates of long bones was also conducted by μCT. As illustrated in Table 2, there were no significant differences between null and control animals.

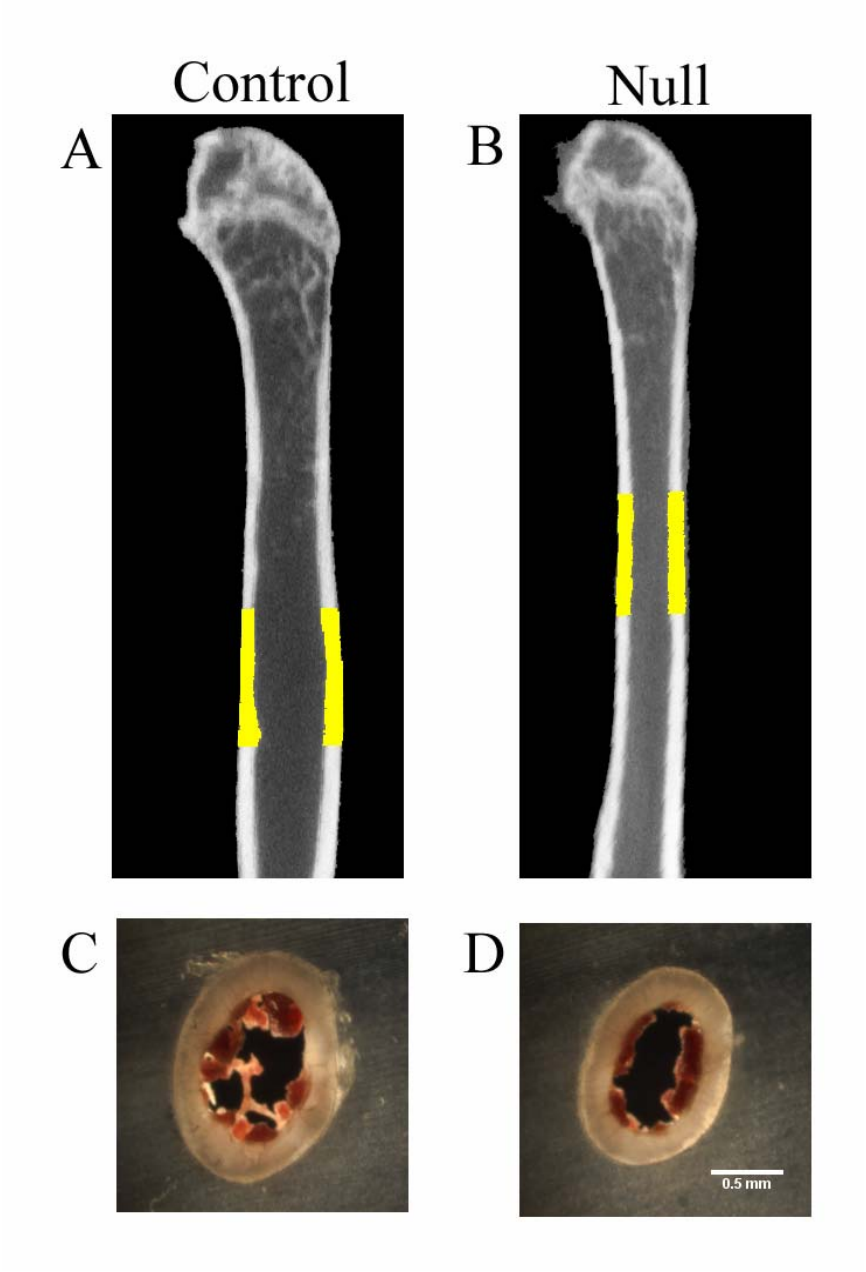

Figure 6: Decreased bone marrow area was apparent in both male and female HIP/RPL29-deficient mice. Radiographs of the femur of control **(A)** and HIP-RPL29-deficient male mice **(B).** The decrease in bone marrow area in mutant animals was obvious in the mid-diaphysis region corresponding to the zone of measurements highlighted in yellow (micro-CT measurements summarized in Table 1). The same observation could be made on mid-shaft cross-sections of adult female femurs obtained after embedding in polymethylmethacrylate (compare WT in **C** to null in **D**).

Table 1: Diaphyseal cortical parameters of six month-old HIP/RPL29-deficient and control male femurs at mid-shaft obtained by μCT

	Control(n=5)	*NULL(n=9)*	*% Reduction*	*p<0.05*
Outer Perimeter (mm)	5.51 +/- 0.477	4.76 +/- 0.212	14.6	+
Inner Perimeter (mm)	3.89 +/- 0.403	3.05 +/- 0.213	22.2	+
Total Tissue Area (mm^2)	2.23 +/- 0.344	1.66 +/- 0.127	26.9	+
Marrow Area (mm^2)	1.08 +/- 0.227 (48.5%)	0.665 +/- 0.093 (40.2%)	39.7	+
Cortical Bone Area (mm^2)	1.15 +/- 0.132 (51.5%)	0.989 +/- 0.066 (59.8%)	15.1	+
Moment of Inertia (mm^4)	0.545 +/- 0.098	0.386 +/- 0.25	30.8	+
BMD	866 +/- 47.2	855 +/- 34.3	0.12	_
BMC	0.019 +/- 0.002	0.017 +/- 0.001	0.02	_

Results are reported as means +/- standard deviation. BMD: bone mineral density, BMC: bone mineral content

Table 2: Trabecular parameters of six month-old HIP/RPL29-deficient and control male distal femora below the growth plate obtained by μCT.

	Control(n=5)	*Null(n=9)*	*p< 0.05*
BV/TV	0.249 +/- 0.034	0.261 +/- 0.069	_
BS/BV	35.4 +/- 1.89	33.3 +/- 6.53	_
Tb. Th. (μm)	56.6 +/- 2.99	61.9 +/- 10.8	_
Tb.Sp. (μm)	174 +/- 32.7	187 +/- 64.6	_
Tb.N.	4.39 +/- 0.575	4.18 +/- 0.839	_
Total Volume (mm^3)	3.18 +/- 0.522	2.21 +/- 0.185	+

Results are reported as means +/- standard deviation. BV: bone volume, BS bone surface, N: number, Sp: spacing Tb: trabecular, Th: thickness, TV: total volume

Histological analysis of femoral heads taken from six month-old female mice also supported findings seen in the trabecular region of male mice. Von Kossa staining did not reveal a decrease in the mineral content of HIP/RPL29-null tissue and supported the data obtained by μCT analysis (Fig. 7). In addition, bones deficient of HIP/RPL29 retained proper growth plate and trabecular bone morphology. Observations of consecutive sections stained by the Goldner's Trichrome method also did not reveal any gross differences in bone microstructure (Fig. 7). Tartrate resistant acid phosphatatse (TRAP) activity was assessed in the proximal growth plate of the tibiae from control and null mice as described in Material and Methods (Fig. 8A). Quantification of TRAP signal in different regions of a section obtained from HIP/RPL29-null mice indicated a modest reduction in osteoclastogenesis and osteoclast activity when compared to a control section (Fig. 8B). The statistical significance of this result will need to be confirmed. Hematoxylin and eosin staining on consecutive sections reveals more organized hypertrophic chondrocytic columns when compared to wild type sections, as well as a thinner growth plate (see arrows in Fig. 9). These observations might be related to a difference in maturity between HIP/RPL29 null and control bones, suggesting a developmental delay persisting in null animals.

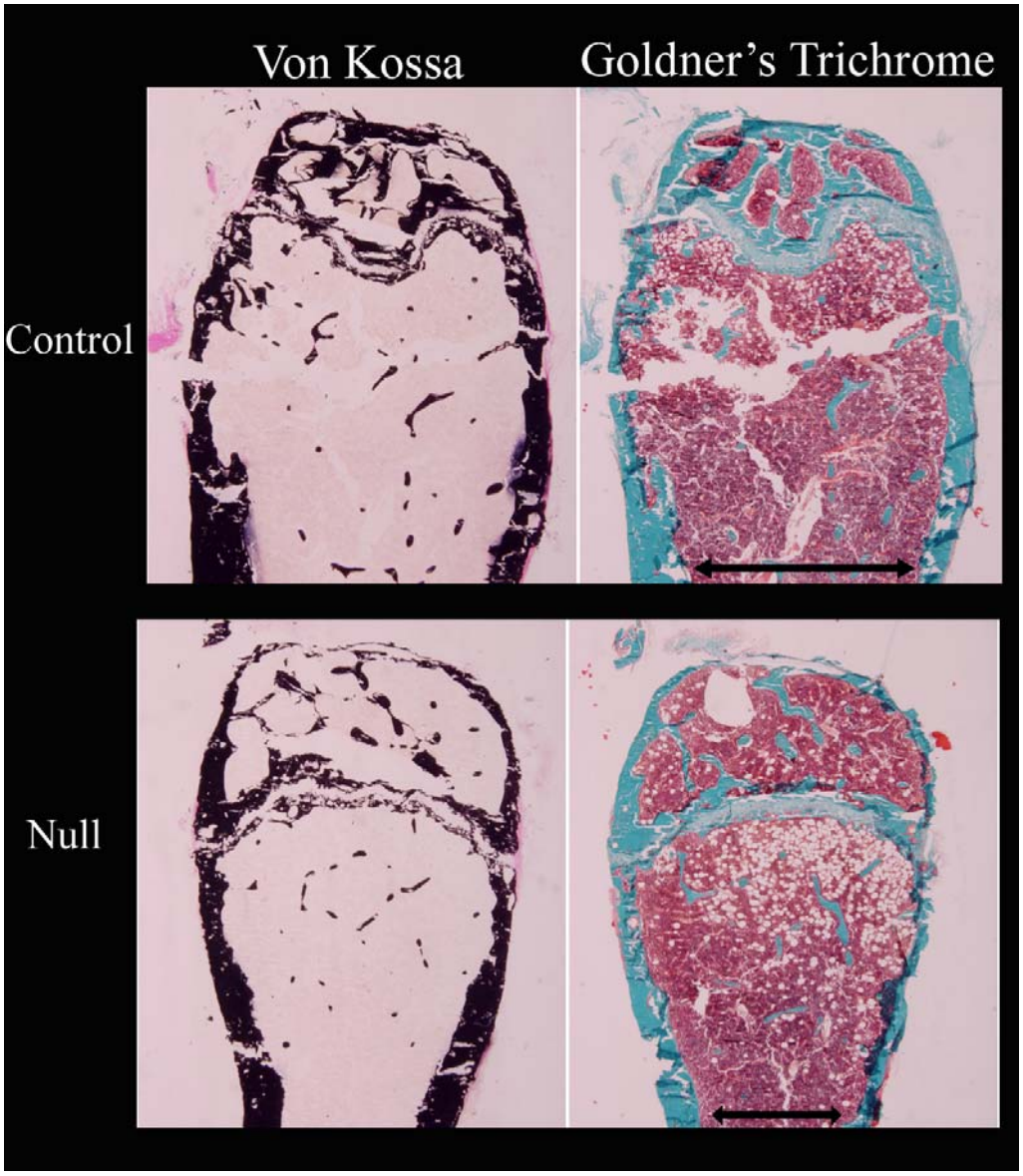

Figure 7: Comparative histology of control and HIP/RPL29-deficient femora. Histological analysis of six-month-old female mice distal femurs showed similar levels of mineralization after detection by Von Kossa staining. Goldner's trichrome staining revealed similar patterning of collagen-rich (green) deposits and comparable growth plate morphologies cellular marrow content (red).

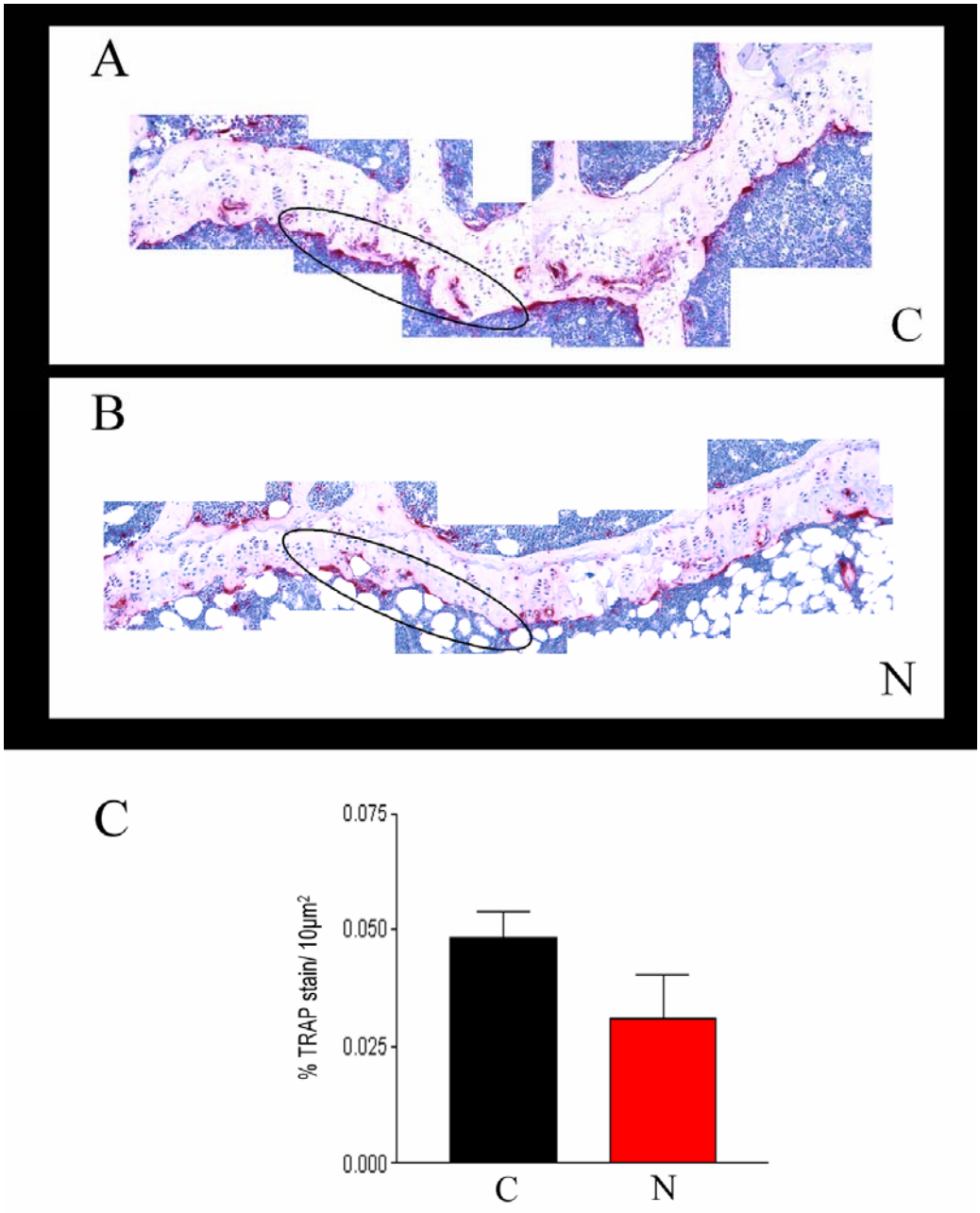

Figure 8: TRAP analysis of the growth plate of six month-old male proximal tibiae. Null animals displayed a moderate reduction in their levels of TRAP activity when compated to wild-type **(compare panel A to panel B)**. Quantification of TRAP signal was analyzed along the curvature of the growth plate which included the calcified cartilage of the growth plate and the upper limits of the primary spongiosa **(C).** Ovals in A and B encompass areas of analysis for each genotype. (n=3)

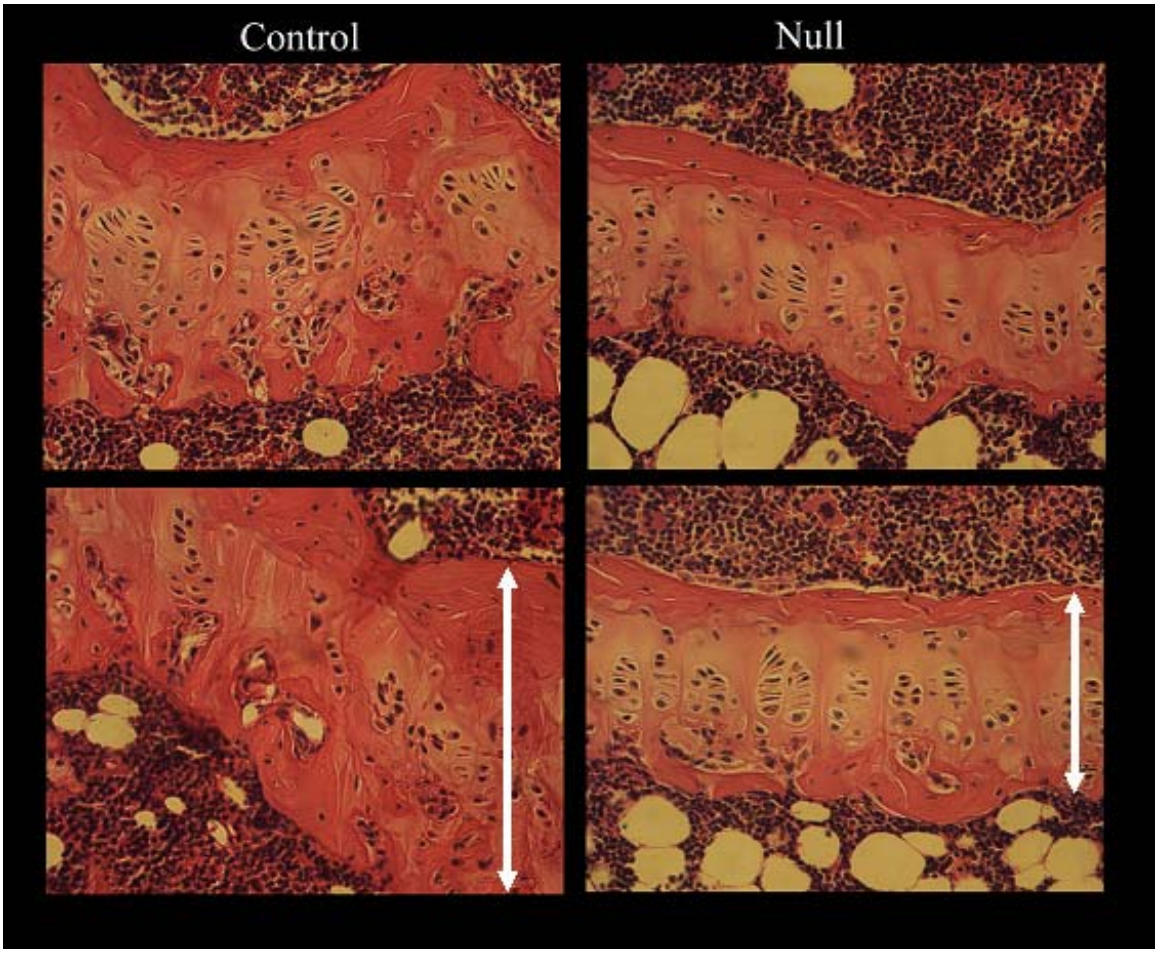

Figure 9: Growth plates of six month-old female tibiae. HIP/RPL29 null display shortened and well organized growth plates (see top and bottom right panels). White arrows clearly demonstrate reduction in growth plate length in HIP/RPL29-deficient bones when compared to control (top and bottom left panels). (Hematoxylin=blue and Eosin=pink)

3.5 Cellular effects of *Hip/Rpl29* gene disruption *in vivo* and *in vitro*

Delayed embryonic development apparent in HIP/RPL29 null mice should also manifest a decrease in growth rate at the cellular level. To test this theory, my colleague and I isolated PMEFs from *Hip/Rpl29*^{tm1Udel} WT, homozygous, and heterozygous embryos, and compared cell size and proliferation rates during their exponential growth. No difference in size between HIP/RPL29 null and wild-type PMEFs was found when observing cells in culture or by flow cytometry (data not shown). HIP/RPL29 null PMEFs proliferated approximately 45% slower than WT controls (Fig. 10, adapted from Kirn-Safran et al., 2007), and heterozygous cultures demonstrated an intermediate proliferation rate with a reduction of approximately 25% when compared with WT controls (Fig. 10). Defects in cell cycle progression also were apparent in null PMEFs after propidium iodide staining and analysis by flow cytometry (data not shown). Results revealed a marked increase in the percentage of null cells with a lower content of DNA, typical of cells arrested in G0/G1 stage of the cell cycle and an almost two-fold decrease in the percentage of cells transitioning into S phase.

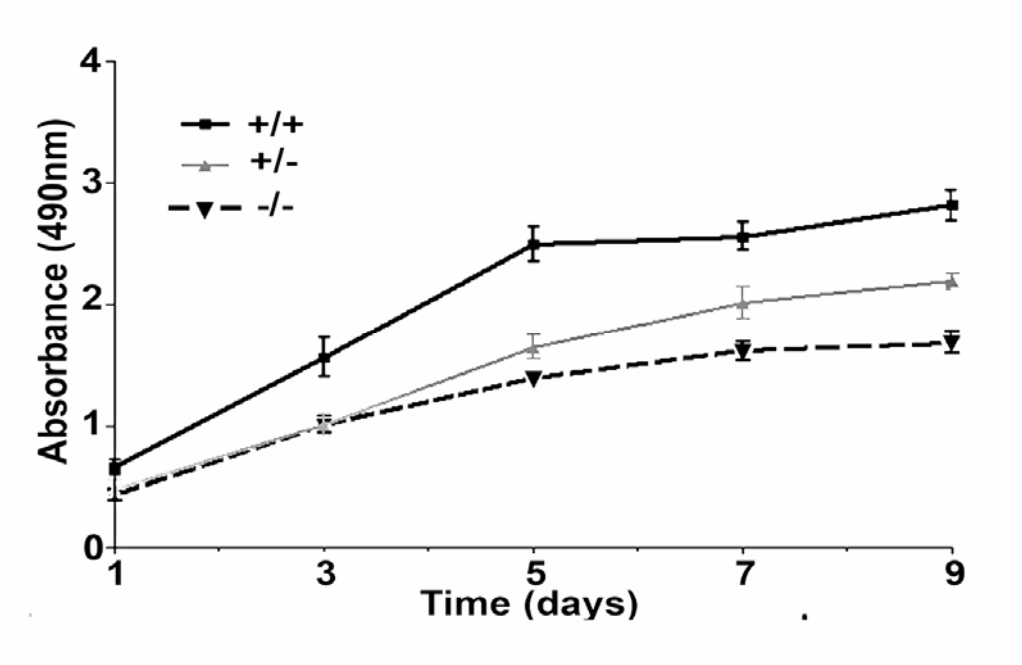

Figure 10: HIP/RPL29-deficient cells display decreased rates of *in vitro* proliferation. PMEFs isolated from HIP/RPL29 null and heterozygous animals proliferated 45% and 25% slower when compared to cells obtained from wild-type animals. Adapted from Kirn-Safran et al., 2007.

Although the epiphysis/growth plate of HIP/RPL29-null day 18.5 embryos were decreased in length (see white double-arrow line), the zone of post-mitotic hypertrophic chondrocytes remained unaffected and no overall alteration of the cartilage growth plate organization was observed when compared with that of WT controls (Fig. 11A&B)**.** Nonetheless, the layer of proliferating (P) chondrocytes was shortened and a significant increase in cellular density could be seen in the reserve zone (R) of null embryos (Fig. 11E, *** $p<0.001$).

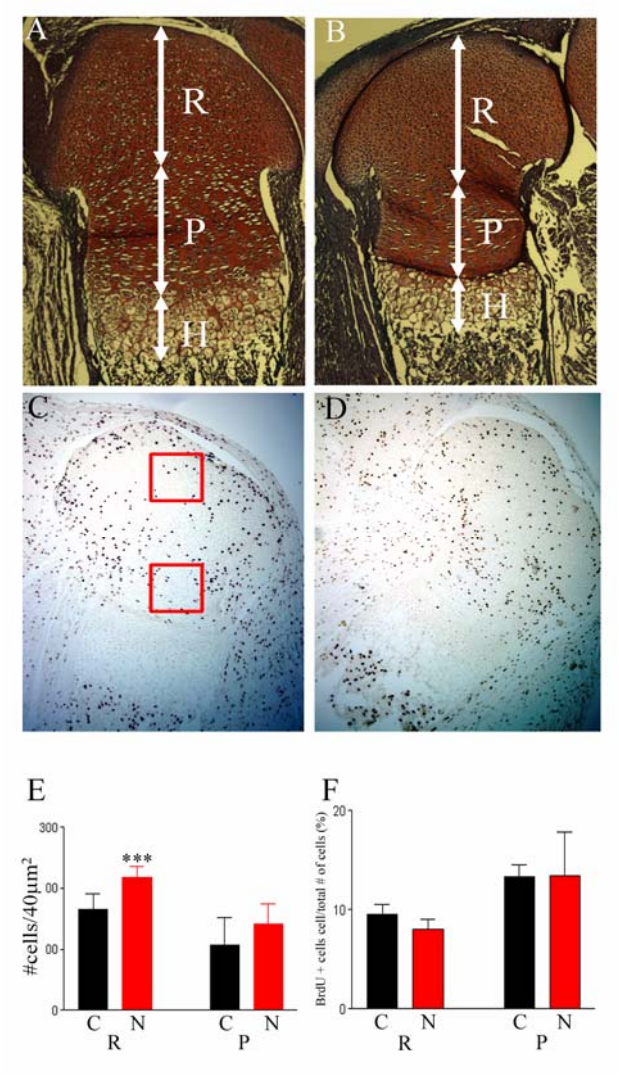

Figure 11: Cell density was increased in the reserve zone of HIP/RPL29$^{-/-}$ embryo distal femoral epiphyses. Although the epiphysis/growth plate of HIP/RPL29-null day 18.5 embryos **(B)** were decreased in length (see white arrows) compared with that of wild-type control **(A)**, no overall alteration of the cartilage growth plate organization was observed using a Safranin-O/Fast green staining method (Red: Safranin-O; Green: Fast Green). However the layer of proliferating (P) chondrocytes was shortened and a significant increase in cellular density could be seen in the reserve zone (R) of null embryos. **(E).** BrdU-labeling did not reveal a significant difference in chondrocyte proliferation in nulls **(D)** compared to wild type **(C)** in either the R or the P zones **(F).** C: control, N: null, ***denotes a statistically significant difference ($p<0.001$) in HIP/RPL29-deficient mice relative to wild type. Red box in C&D illustrates 40µm^2 areas counted and reported in F.

In yeast, the depletion of HIP/RPL29 ortholog leads to decreased levels of translation, ultimately affecting proliferation (DeLabre et al., 2002). To determine if this phenomenon was also apparent in our HIP/RPL29 knockout mice line during chondrocyte differentiation and growth plate development, I conducted *in vivo* proliferation assays. As described in Materials and Methods, proliferation of chondrogenic progenitors and chondrocytes was assessed following intraperitoneal injection of BrdU into day 18.5 pregnant mice by measuring BrdU incorporation into replicating cells in developing embryonic hindlimbs. I concentrated on the epiphyseal growth plate in femoral heads of long bones isolated from developing embryos. HIP/RPL29 wild-type and null embryos displayed similar patterns of BrdU staining and did not show any differences in the number of BrdU positive cells present in the reserve (R) and proliferative (P) zones of the growth plate (Fig. 11C&D), suggesting that the reduction in the epiphyseal growth plate length might not be caused by a defect in the rate of chondrocyte proliferation (Fig. 11F).

3.6 Lack of HIP/RPL29 impairs protein translation

My colleagues and I examined the global protein synthesis rate in WT and null PMEFs by evaluating the incorporation of ^{35}S-labeled methionine/cysteine into cellular proteins to further investigate the cellular effect of *Hip/Rpl29* loss-of-function mutation (Fig. 12A, adapted from Kirn-Safran et al., 2007). An estimated 30% reduction in the rate of protein synthesis was apparent in HIP/RPL29 null cultures when compared with WT cultures. This global reduction of protein synthesis in HIP/RPL29-depleted PMEFs

may be consistent withHIP/RPL29 acting as an accessory protein for translation efficiency and ribosome biogenesis. To test this hypothesis, I investigated the effects of HIP/RPL29 depletion on two other ribosomal proteins, RPS6 and RPL17, belonging to the small and the large subunits, respectively.

The constitutive and phosphorylated, active levels of RPS6, a core component of the 40S subunit, was diminished by approximately 60% in HIP/RPL29 null PMEFs when compared with WT control cells, under both asynchronous and serum-starved and re-fed culture conditions (Fig. 12B and data not shown). However, a reduction of RPS6 protein could not be observed *in vivo* (data not shown) in developing HIP/RPL29-deficient embryos. Evaluation of S6 kinase (S6K) did not reveal a reduction in the steady state or activated levels (Fig. 12C and data not shown), suggesting the reduction in activated levels of RPS6 in HIP/RPL29 null PMEFs, is related to steady state levels of RPS6. In contrast to RPS6, only a small decrease in the steady state level of a structural protein of the large subunit, RPL17, was observed in HIP/RPL29 null cells when compared with its level in WT controls (Fig. 12D). I also did not observe any differences in the steady state or activated levels of the translation initiation factor eIF4G (Fig. 12E), suggesting the apparent defect in global protein synthesis may be related to availability of ribosomal components and subsequent ribosome biogenesis and not initiation of protein translation (Kirn-Safran et al., 2007).

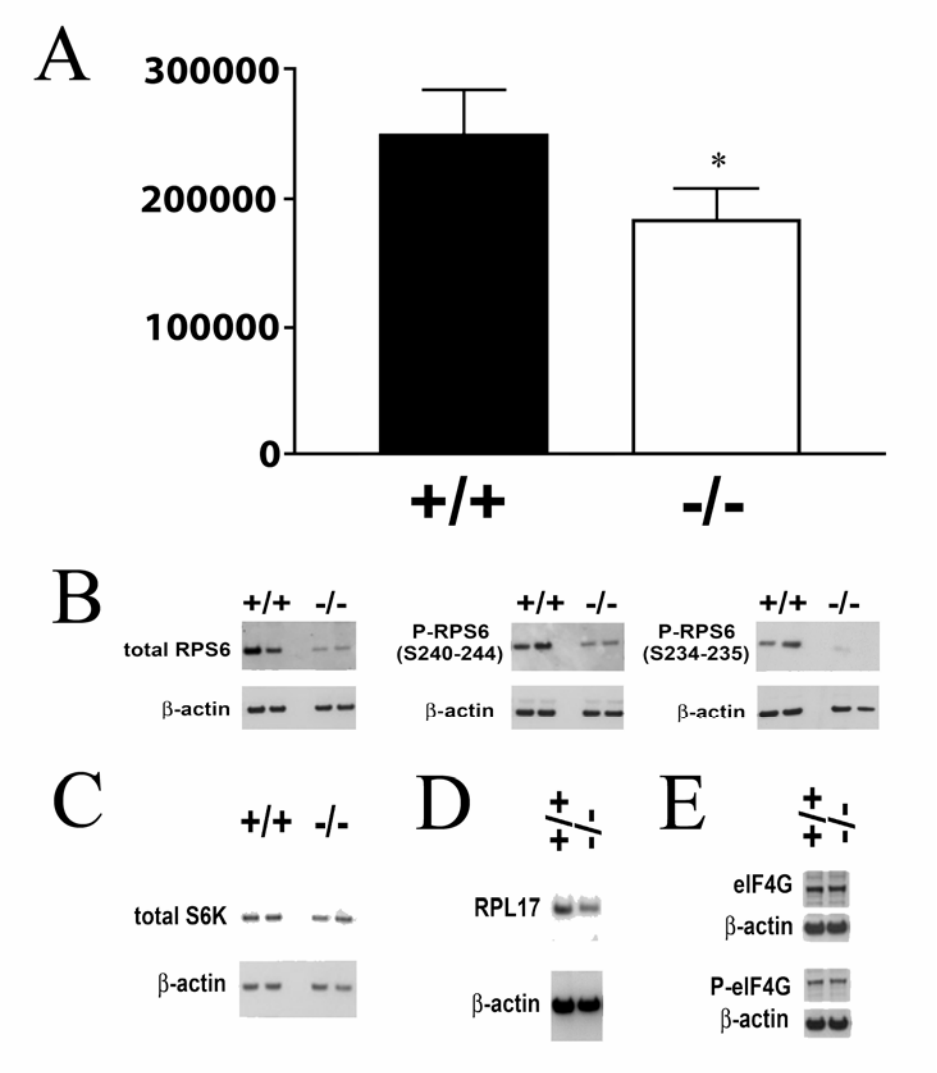

Figure 12: HIP/RPL29 deletion resulted in reduction of core ribosomal components, decreasing overall translation. Global protein synthesis, analyzed by [^{35}S] cysteine and [^{35}S] methione incorporation, revealed a significant decrease in global translation rate in HIP/RPL29 null PMEFs when compared to wild-type (+/+) **(A)**. Western blot analysis of protein extracts obtained from wild type and HIP/RPL29 null PMEFs (**B, C, D**, and **E**). There was an apparent decrease in the steady state RPS6 and activated levels (S6) of core ribosomal component **(B)**. Although not as pronounced, I also saw a decrease in the steady state levels of RPL17 (**D**). eIF4G, a factor necessary for cap-dependent translation initiation, was not reduced in HIP/RPL29 null PMEFs compared to control cells (**E**). *: $p<0.01$

Chapter 4

DISCUSSION

4.1 Global skeletal defects in HIP/RPL29 null mice

The short stature phenotype of HIP/RPL29 null mice manifests itself from pre- and postnatal life into adulthood (Kirn-Safran et al., 2007). A reduction in total body size seen in pre- and postnatal embryos is not overcome as HIP/RPL29 mice enter puberty and grow into adulthood. At six months of age the long bones of null mice continue to display significant reductions in overall bone length and wet weight. Thus, embryonic growth delay resulted in considerable differences in overall skeletal size and weight when comparing WT and HIP/RPL29 null animals.

Bones deficient of HIP/RPL29 protein also reveal differences in bone geometry in a site specific manner. The femoral mid-diaphysis of six-month old HIP/RPL29 null males contains less cortical bone tissue and reveal alterations in its distribution when compared to age-matched WT mice. In addition, no apparent histological variation besides reduction of the overall space occupied by the tissue was observed in the trabecular bone region of the distal head of the femur. The total amount, distribution, and organic and inorganic content of bone tissues are responsible for predicting strength and toughness of bone (Jepsen et al., 2002). Similar levels of BMD and BMC in HIP/RPL29-deficient and

control bones predict the amount of stress these bones can withstand will be equivalent; however the organization and content of collagen or other non-collagenous proteins are unknown at this time. Reduction of collagen content in HIP/RPL29 null bones, due to inefficiencies seen in protein translation, will decrease the elastic properties of the bone causing the bone to bend and break with less force. This would be an important factor to investigate if fracture studies indicate a reduction in HIP/RPL29 null bone strength. On the other hand, the diminished polar moment of inertia reported in HIP/RPL29-deficient bones, predict these bones will deform and subsequently fracture under lower torsional strains when compared to controls.

It also has been reported for different strains of mice that genotype-specific variations in postnatal, pubertal, and post-pubertal growth patterns and mineral accrual explain differences in adult bone trait combinations and, thus, bone fragility (Price et al., 2005). These data support this idea; the genetic variation between WT and HIP/RPL29 null mice manifests itself in an overall growth and development defect. Thus, this defect is responsible for the differences seen in the bone geometry when comparing WT and HIP/RPL29-deficient bones.

Variations in bone microstructure and bone mineral density have been associated with sex, as well, as age. Cyclooxygenase-2 (COX-2) null mice manifest different skeletal phenotypes in responses to gene knockout when comparing males and females. Male $COX2^{-/-}$ mice display a larger volume of cortical bone that is well structured when

compared to female COX2$^{-/-}$ mice. Females COX2$^{-/-}$ female mice, on the other hand, have smaller less structured cortical bone, with a higher BMD then male knockout mice (Robertson et al., 2006). Age matched HIP/RPL29 null female mice, display almost identical relative reductions in overall bone length and weight when compared to age matched male mice. Analysis of cross-sections of HIP/RPL29-deficient femurs in female mice at mid-shaft show reductions in marrow and total tissue area consistent with μCT data obtained for HIP/RPL29 null male femurs. Likewise, histological observation of the trabecular region in female mouse femurs revealed an architecture similar to the one observed by μCT x-ray radiographs. Therefore, no major difference in the bone phenotype seen in male and female HIP/RPL29 null mice is anticipated. Further analysis of femurs from six-month-old WT and HIP/RPL29 female mice by μCT must be carried out to verify this hypothesis.

4.2 *In vivo* and *in vitro* cellular effects of HIP/RPL29 protein deletion

The coordinated proliferation, hypertrophy, and apoptosis of chondrocytes that occurs during both embryonic long bone development and adult bone growth (Olsen et al., 2000, Woods et al., 2007), serve as great systems for the investigation of biological mechanisms that lie at the heart of the growth delay and skeletal phenotype seen in HIP/RPL29 null mice. *In vitro* analysis using PMEFs indicated a significant decrease in the proliferation rate when comparing HIP/RPL29 null and WT cells, however the proliferative potential of chondrogenic progenitors and chondrocytes *in vivo* was

unaffected by deletion of HIP/RPL29 protein. This suggests compensatory mechanisms which act to correct for the loss of HIP/RPL29 *in vivo.*

When comparing growth plate morphology of HIP/RPL29 null embryos to controls, a reduction in the length of the chondrocytic proliferative zone was seen in null animals. This observation is most likely related more to cell-cycle defects as opposed to proliferation. It is well known that a decrease in the size of the proliferative zone of the growth plate results either from a delay in differentiating from reserve into proliferative chondrocytes or from accelerated terminal differentiation into hypertrophic chondrocytes. Because HIP/RPL29 null mice display an increase of cell density in the reserve zone of the growth plate, my colleagues and I believe that reduction in the overall number of dividing chondrocytes is due to the delayed entry of their progenitors into the cell cycle. In accordance with this idea, the hypertrophic zone in HIP/RPL29-deficient hindlimbs does not display a reduction in size when compared to controls. Furthermore, the consequences of this defect are still visible in adult HIP/RPL29-null growth plates. Consistent with these results, defects in cell cycle progression were observed in both HIP/RPL29 null PMEFs and PMEFs heterozygous for RPL24 issued from another mouse model which displays a short stature phenotype (Kirn-Safran et al., 2007, Oliver et al., 2004). The proliferative activity in hindlimbs was analyzed *in vivo* during the later stages of long bone development (day 18.5), greater alterations in both proliferation and cell cycle progression may be apparent at earlier stages of cartilage and bone development and should be further investigated.

4.3 Protein translational efficiency was compromised in HIP/RPL29-deficent cells

In vitro data suggests HIP/RPL29, a component of actively translating ribosomes, may act as an accessory ribosomal protein increasing translation efficiency during times of active cell growth (Kirn-Safran et al., 2007). Analysis of PMEFs isolated from WT heterozygous, and null embryos displayed decreased rates of proliferation and global protein synthesis in HIP/RPL29-deficient cells. The approximate 30% decrease seen in global protein translation is similar to levels seen in mouse embryos or *Minute Drosophila* mutants with defects in riboproteins (Boring et al., 1989, Oliver et al., 2004). DeLabre et al. (2002) also reported a 50% decrease in global protein synthesis in a RPL29 mutant yeast strain.

Lack of HIP/RPL29 also impaired the steady state levels of other ribosomal proteins, RPS6 and RPL17. *In vitro* studies have shown RPS6 is located on the small ribosomal subunit interface (Nika et. al, 1984), a region HIP/RPL29 is also believed to colocalize during the bridging of the large and small ribosomal subunits (Nygard et. al, 1990), my colleagues and I hypothesize that RPS6 serves as a docking site for the large ribosomal subunit, where HIP/RPL29 will bind and aid in the stabilization the bridging of the 40S and 60S interface. This implies a crucial role for HIP/RPL29 in the assembly and generation of active ribosomes. These data, and preliminary results, also reveal a reduction in the steady state levels of RPL17, as well as a decrease in the total content of 28S rRNA. Altogether, these data reveal a defect in the production and maintenance of

core ribosomal components in HIP/RPL29-deficient cells. Polysomal fractionation on continuous sucrose gradients need to be carried out to confirm this hypothesis.

In support of data presented above, lack of RPS19 *in vitro* displayed a defect in the synthesis and maintenance of 18S rRNA followed by defects in ribosome biogenesis (Choesmel et al., 2006). In conjunction, RPS19 depletion produced a reduction in steady-state levels of RPS6 and RPS16 via a post-transcriptional mechanism while the levels of large RPs were unaltered, supporting the idea that levels of RPs are determined by subunit assembly (Idol et al., 2007). However, studies in yeast systems have shown that depletion of one RP does not result in the reduced production of other RPs, but proposes ribosomal components that are not assembled into ribosome are rapidly degraded (Idol et al., 2007). Therefore, it is possible that the lack of HIP/RPL29 affects the assembly and/or stability of both ribosomal subunits resulting in decreases of ribosomal components for both the 40S and 60S ribosomal subunits (RPs and 28S rRNA) due to the rapid degradation of free components. This will ultimately affect the number of available ribosomes capable of translating proteins. Recent *in vitro* preliminary results indicate that HIP/RPL29-deficient cells contain less active ribosome than WT cells, indicating a decrease in the capacity for protein synthesis by these cells

Defects in ribosome biogenesis could change the accuracy of translation and alter developmental cues (Panic et al., 2006). This idea may help to explain both cellular and growth defects seen in HIP/RPL29 null mice. Without the required levels of cytosolic and extracellular proteins, biological mechanisms controlling cellular growth and

differentiation cannot function properly. Thus, cells are forced to "wait" until sufficient steady-state levels are accrued. Delays in the cell cycle progression of HIP/RPL29 null cells *in vivo* and *in vitro* also can be explained by this idea. Decreases in ECM components may alter cell-cell and cell-ECM interactions, affecting cell morphologies, signaling capabilities, and differentiation potential. Because global translational efficiency also is reduced by deletion of HIP/RPL29 protein, it is possible the reduced size of the epiphyseal growth plate in null embryos is caused by reduced matrix volume. This deficiency also could potentially alter the structural integrity of the ECM.

4.4 Conclusions

In regard to bone development and maintenance, decreased rates of proteins synthesis would compromise events important for maintaining cellular processes. The cartilage scaffold would form more slowly and not be as structurally sound. On the other hand, the delayed production of osteoblasts and impaired function due to reduced protein synthesis also may have detrimental effects on the structural properties and mechanics of bone tissue. BMD and BMC in HIP/RPL29 null mice femur are comparable to measurements obtained from WT samples; however, these measurements do not reveal any information about the organic, collagenous properties of the bone. Alterations in overall content and organization are potential candidates for not only determining the amount of bone tissue, but also its structural properties. The coupling and cooperative interactions of these organic bone components in combination with mineralized cartilage provide a stiff structure capable of withstanding high forces before fracture (Gupta et al.,

2005). Defects in bone geometry and distribution will cause reductions in bone toughness. Future studies using three-point bending will aid in determining the biomechanical properties of HIP/RPL29-deficient bones relative to controls.

Deletion of RPL19 and L24, as well as heterozygosity of RPS6 in inbred mouse models, all resulted in prenatal lethality (Matsson et al., 2004, Oliver et al., 2004, Panic et al., 2006). Unlike mutations or deletion of other RPs, *in vivo* compensatory mechanisms must exist to correct for the loss of HIP/RPL29. However these mechanisms are not sufficient to overcome the growth delays seen in HIP/RPL29-deficient animals. In conclusion, these data suggest loss of HIP/RPL29 *in vitro* results in altered ribosome biogenesis, decreasing global protein synthesis and cell cycle progression. Altered rate of protein accrual affects the overall differentiation and subsequent function of cellular processes. Delays at the cellular levels manifest themselves *in vivo* through further delays in tissue development, ultimately affecting the entire organism, both early and later in life. Global growth delays in HIP/RPL29 mice due to delays in cellular function, results in a short stature, skeletal phenotype with decreased bone quantity, distribution, and potentially quality. My colleagues and I hypothesize these alterations will result in decreased bone strength and rigidity.

REFERENCES

Aszodi A., J.F. Bateman, E. Gustafsson, R. Boot-Handford, R. Fassler (2000). "Mammalian skeletogenesis and extracellular matrix: what can we learn from knockout mice?" Cell Struct Funct. 25(2):73-84.

Boring L. F., B. Sinervo, G. Schubiger (1989) "Experimental phenocopy of a minute maternal-effect mutation alters blastoderm determination in embryos of Drosophila melanogaster." Dev Biol. 132(2):343-54.

Brodersen D. E., P. Nissen (2005). "The social life of ribosomal proteins." FEBS J. 272(9):2098-108.

Choesmel V., D. Bacqueville, J. Rouquette, J. Noaillac-Depeyre, S. Fribourg, A. Cretien, T. Leblanc, G. Tchernia, L. Da Costa, P.E. Gleizes (2007). "Impaired ribosome biogenesis in Diamond-Blackfan anemia." Blood. 109(3):1275-83.

Costell M., E. Gustafsson, A. Aszodi, M. Morgelin, W. Bloch, E. Hunziker, K. Addicks, R. Timpl, R. Fassler (1999). "Perlecan maintains the integrity of cartilage and some basement membranes." J Cell Biol. 147(5):1109-22.

DeLabre M. L.,J. Kessl, S. Karamanou, B.L. Trumpower (2002) "RPL29 codes for a non-essential protein of the 60S ribosomal subunit in Saccharomyces cerevisiae and exhibits synthetic lethality with mutations in genes for proteins required for subunit coupling." Biochim Biophys Acta. 12;1574(3):255-61.

de Nigris F., R. Visconti, J. Cerutti, D. Califano, A Mineo, M. Santoro, G. Santelli, A. Fusco (1998) "Overexpression of the HIP gene coding for a heparin/heparan sulfate-binding protein in human thyroid carcinomas." Cancer Res. 58(20):4745-51.

Dempster, D., "Anatomy and Function of the Adult Skeleton." Primer on the Metabolic Bone Diseases and Disorders of Mineral Metabolism. Ed. M J. Favus. American Society for Bone and Mineral Research, 2006. 7-11.

Dixon J, N. C. Jones, L. L. Sandell, S. M. Jayasinghe, J. Crane, J. P. Rey, M. J. Dixon, P. A. Trainor (2006). "Tcof1/Treacle is required for neural crest cell formation and proliferation deficiencies that cause craniofacial abnormalities." Proc Natl Acad Sci U S A. 103(36):13403-8.

Dong J., R. Lai, K. Nielsen, C.A. Fekete, H. Qiu, A.G. Hinnebusch (2004). "The essential ATP-binding cassette protein RLI1 functions in translation by promoting preinitiation complex assembly". J Biol Chem. 279(40):42157-68.

Farach M. C., J. P. Tang, G. L. Decker, D. D. Carson (1987). Heparin/heparin sulfate is involved in attachment and spreading of mouse embryos *in vitro*." Dev. Biol. 123(2):401-10.

Fatica A., D. Tollervey (2002) "Making ribosomes." Curr Opin Cell Biol. 14(3):313-8.

Fritsch A., C. Hellmich (2007) "'Universal' microstructural patterns in cortical and trabecular, extracellular and extravascular bone materials: micromechanics-based prediction of anisotropic elasticity." J Theor Biol. 244(4):597-620.

Fromont-Racine M., B. Senger, C. Saveanu, F. Fasiolo (2003). "Ribosome assembly in eukaryotes." Gene. 313:17-42.

Gupta H. S., W Wagermaier, G.A. Zickler, D. Raz-Ben Aroush, S.S. Funari, P Roschger, H.D. Wagner, P. Fratzl (2005). "Nanoscale deformation mechanisms in bone." Nano Lett. 5(10):2108-11.

Hedges J., M. West, A.W. Johnson (2005). "Release of the export adapter, Nmd3p, from the 60S ribosomal subunit requires Rpl10p and the cytoplasmic GTPase Lsg1p." EMBO J. 9;24(3):567-79.

Hoke D. E., E.G. Regisford, J. Julian, A. Amin, C. Begue-Kirn, D.D. Carson (1998). "Murine HIP/L29 is a heparin-binding protein with a restricted pattern of expression in adult tissues." J Biol Chem. 273(39):25148-57.

Idol R. A., S. Robledo, H. Y. Du, D. L. Crimmins, D. B. Wilson, J.H. Ladenson, M. Bessler, P.J. Mason (2007). "Cells depleted for RPS19, a protein associated with Diamond Blackfan Anemia, show defects in 18S ribosomal RNA synthesis and small ribosomal subunit production." Blood Cells Mol Dis. 39(1):35-43.

Jepsen K. J., O.J. Akkus, R. J. Majeska, J. H. Nadeau (2003). "Hierarchical relationship between bone traits and mechanical properties in inbred mice." Mamm Genome. 14(2):97-104.

Julian J., S.K. Das, S. K. Dey, D. Baraniak, V.T. Ta, D.D. Carson (2001). "Expression of heparin/heparan sulfate interacting protein/ribosomal protein l29 during the estrous cycle and early pregnancy in the mouse." Biol Reprod. 64(4):1165-75.

Kirn-Safran C. B., S. Dayal, P.A. Martin-DeLeon, D. D. Carson (2000). "Cloning, expression, and chromosome mapping of the murine Hip/Rpl29 gene." Genomics. 68(2):210-9.

Kirn-Safran C. B., J Julian, J. E. Fongemie, D. E. Hoke, K. J. Czymmek, D. D. Carson (2002). "Changes in the cytologic distribution of heparin/heparan sulfate interacting protein/ribosomal protein L29 (HIP/RPL29) during *in vivo* and *in vitro* mouse mammary epithelial cell expression and differentiation." Dev Dyn. 223(1):70-84.

Kirn-Safran C. B., D. S. Oristian, R. J. Focht, S. G. Parker, J. L. Vivian, D. D. Carson (2007). "Global growth deficiencies in mice lacking the ribosomal protein HIP/RPL29." Dev Dyn. 236(2):447-60.

Kispal G., K. Sipos, H. Lange, Z. Fekete, T. Bedekovics, T. Janaky, J. Bassler, D. J. Aguilar Netz, J. Balk, C. Rotte, R. Lill (2005). "Biogenesis of cytosolic ribosomes requires the essential iron-sulphur protein Rli1p and mitochondria." EMBO J. 24(3):589-98.

Kline, K. (1955). "The Microtomist's Formulary and Guide." Am J Public Health Nations Health. 45(1): 111.

Laine RO, Laipis PJ, Shay NF, Kilberg MS. (1991). "Identification of an amino acid-regulated mRNA from rat liver as the mammalian equivalent of bacterial ribosomal protein L22." J Biol Chem. 266(26):16969-72.

Koller D. L., J. Schriefer, Q. Sun, K. L. Shultz, L. R. Donahue, C. J. Rosen, T. Foroud, W. G. Beamer, C. H. Turner (2003). "Genetic effects for femoral biomechanics, structure, and density in C57BL/6J and C3H/HeJ inbred mouse strains." J Bone Miner Res. 18(10):1758-65.

Laine R. O., P. J. Laipis, N. F. Shay, M. S. Kilberg (1991). "Identification of an amino acid-regulated mRNA from rat liver as the mammalian equivalent of bacterial ribosomal protein L22." J Biol Chem. 266(26):16969-72.

Ling Y., H. F. Rios, E. R. Myers, Y. Lu, J. Q. Feng, A. L. Boskey (2005). "DMP1 depletion decreases bone mineralization *in vivo*: an FTIR imaging analysis." J Bone Miner Res. 20(12):2169-77.

Liu S., F. Zhou, M. Hook, D. D. Carson (1997). "A heparin-binding synthetic peptide of heparin/heparan sulfate-interacting protein modulates blood coagulation activities." Proc Natl Acad Sci U S A. 94(5):1739-44.

Liu J. M., S. R. Ellis (2006). "Ribosomes and marrow failure: coincidental association or molecular paradigm?" Blood. 107(12):4583-8.

Lowry O. H., N. J. Rosebrough, A. L. Farr, R. J. Randall. (1951). "Protein measurement with the Folin phenol reagent." J Biol Chem. 193(1):265-75.

Marchetti D., S. Liu, W. C. Spohn, D. D. Carson (1997). "Heparanase and a synthetic peptide of heparan sulfate-interacting protein recognize common sites on cell surface and extracellular matrix heparan sulfate." J Biol Chem. 272(25):15891-7.

Matsson H., E. J. Davey, N. Draptchinskaia, I. Hamaguchi, A. Ooka, P. Leveen, E. Forsberg, S. Karlsson, N. Dahl (2004). "Targeted disruption of the ribosomal protein S19 gene is lethal prior to implantation." Mol Cell Biol. 24(9):4032-7.

Miller S. A., A. J. Brown, M. C. Farach-Carson, C. B. Kirn-Safran (2003). "HIP/RPL29 down-regulation accompanies terminal chondrocyte differentiation." Differentiation. 71(6):322-36.

Mundlos S., B. R. Olsen (1997). "Heritable diseases of the skeleton. Part I: Molecular insights into skeletal development-transcription factors and signaling pathways." FASEB J. 11(2):125-32.

Mundlos S., B. R. Olsen (1997). "Heritable diseases of the skeleton. Part II: Molecular insights into skeletal development-matrix components and their homeostasis." FASEB J. 11(4):227-33

Nika H., T. Hultin (1984). "Location of the sulfhydryl groups involved in disulfide interaction between the neighboring proteins L6 and L29 in mammalian ribosomes. S-cleavage of the cyanylated proteins in polyacrylamide gels after separation by dodecylsulfate gel electrophoresis." Eur J Biochem. 142(3):521-6.

Nagy A., M. Gertsenstein, K Vintersten, R. Behringer (2003). Manipulating the mouse embryo. Cold Spring Harbor, NY: Cold Spring Harbor Laboratory Press. p.764

Nygard O., L. Nilsson (1990). "Translational dynamics. Interactions between the translational factors, tRNA and ribosomes during eukaryotic protein synthesis." Eur J Biochem. 191(1):1-17.

Oliver E. R., T. L. Saunders, S. A. Tarle, T Glaser (2004). "Ribosomal protein L24 defect in belly spot and tail (Bst), a mouse Minute." Development. 131(16):3907-20.

Olsen B. R., A. M. Reginato, W Wang. (2000). "Bone development." Annu Rev Cell Dev Biol. 16:191-220.

Panic L., S. Tamarut, M. Sticker-Jantscheff, M. Barkic, D. Solter, M. Uzelac, K. Grabusic, S. Volarevic (2006). "Ribosomal protein S6 gene haploinsufficiency is associated with activation of a p53-dependent checkpoint during gastrulation." Mol Cell Biol. 26(23):8880-91.

Pestov D. G., Z. Strezoska, L. F. Lau (2001). "Evidence of p53-dependent cross-talk between ribosome biogenesis and the cell cycle: effects of nucleolar protein Bop1 on G(1)/S transition." Mol Cell Biol. 21(13):4246-55.

Price C., B. C. Herman, T. Lufkin, H. M. Goldman, K. J. Jepsen (2005). "Genetic variation in bone growth patterns defines adult mouse bone fragility. J Bone Miner Res. 20(11):1983-91.

Raught B., A. C. Gingras, S. P. Gygi, H. Imataka, S. Morino, A. Gradi, R. Aebersold, N. Sonenberg (2000). "Serum-stimulated, rapamycin-sensitive phosphorylation sites in the eukaryotic translation initiation factor 4GI." EMBO J. 19(3):434-44.

Rho J. Y., L. Kuhn-Spearing, P. Zioupos (1998). "Mechanical properties and the hierarchical structure of bone." Med Eng Phys. 20(2):92-102.

Robertson E.J. Teratocarcinomas and embryonic stem cells a practical approach. Oxford, Washington, DC: IRL Press. 1987. p.254

Robertson G., C. Xie, D. Chen, H. Awad, E. M. Schwarz, R. J. O'Keefe, R. E. Guldberg, X. Zhang. (2006). "Alteration of femoral bone morphology and density in COX-2-/- mice. Bone. 39(4):767-72.

Rohde L. H., J. Julian, A. Babaknia, D. D. Carson (1996). "Cell surface expression of HIP, a novel heparin/heparan sulfate binding protein, of human uterine epithelial cells and cell lines." J Biol Chem. 271(20):11824-30.

Rohde L. H., M. J. Janatpore, M. T. McMaster, S. Fisher, Y. Zhou, K. H. Lim, M. French, D. Hoke, J. Julian, D. D. Carson (1998). "Complementary expression of HIP, a cell-surface heparan sulfate binding protein, and perlecan at the human fetal-maternal interface." Biol Reprod. 58(4):1075-83.

Rubin C., J. Rubin. "Biomechanics and Mechanobiology of Bone." Primer on the Metabolic Bone Diseases and Disorders of Mineral Metabolism. Ed. M J. Favus. American Society for Bone and Mineral Research, Washington D.C. 2006. p. 36-42.

Sawyer A., P. Lott, J. Titrud, J.J. McDonald (2003). "Quantification of tartrate resistant acid phosphatase distribution in mouse tibiae using image analysis." Biotech Histochem. 78(5):271-8.

Schmidt E. V. (1999). "The role of c-myc in cellular growth control." Oncogene. 13;18(19):2988-96.

Tschochner H., E. Hurt (2003) "Pre-ribosomes on the road from the nucleolus to the cytoplasm." Trends Cell Biol. 13(5):255-63.

Wang Y., D. Cheong, S. Chan, S. C. Hooi (1999). "Heparin/heparan sulfate interacting protein gene expression is up-regulated in human colorectal carcinoma and correlated with differentiation status and metastasis." Cancer Res. 59(12):2989-94.

Woods A., G. Wang, F. Beier (2007). "Regulation of chondrocyte differentiation by the actin cytoskeleton and adhesive interactions." J Cell Physiol. Published online May 10.

Wool I. G. (1996). "Extraribosomal functions of ribosomal proteins." Trends Biochem Sci. 21(5):164-5.

Yang X, K. Matsuda, P. Bialek, S. Jacquot, H. C. Masuoka, T. Schinke, L. Li, S. Brancorsini, P. Sassone-Corsi, T. M. Townes, A. Hanauer, G. Karsenty (2004). "ATF4 is a substrate of RSK2 and an essential regulator of osteoblast biology; implication for Coffin-Lowry Syndrome." Cell. 117(3):387-98.

Yeo H., L. H. Beck, J. M. McDonald, M. Zayzafoon (2007). "Cyclosporin A elicits dose-dependent biphasic effects on osteoblast differentiation and bone formation." Bone. 40(6):1502-16.

Zheng J. Q., T. K. Kelly, B. Chang, S. Ryazantsev, A. K. Rajasekaran, K. C. Martin, J. L. Twiss (2001) "A functional role for intra-axonal protein synthesis during axonal regeneration from adult sensory neurons." J Neurosci. 21(23):9291-303.